Journal Pre-proof

Piezoelectric-piezomagnetic behaviour of coated long fiber composites accounting for eigenfields

George Chatzigeorgiou, Adil Benaarbia, Fodil Meraghni

PII: S0167-6636(19)30550-2
DOI: https://doi.org/10.1016/j.mechmat.2019.103157
Reference: MECMAT 103157

To appear in: *Mechanics of Materials*

Received date: 28 June 2019
Revised date: 26 August 2019
Accepted date: 27 August 2019

Please cite this article as: George Chatzigeorgiou, Adil Benaarbia, Fodil Meraghni, Piezoelectric-piezomagnetic behaviour of coated long fiber composites accounting for eigenfields, *Mechanics of Materials* (2019), doi: https://doi.org/10.1016/j.mechmat.2019.103157

Highlights

- Micromechanical approach to evaluate the electro-magneto-inelastic properties in coated long fiber composites with transversely isotropic piezoelectric-piezomagnetic behaviour
- Composite Cylinders Assemblage type of boundary conditions to obtain analytical expressions of the dilute electro-magneto-mechanical concentration tensors
- Mori-Tanaka is adapted to identify i) the overall response of the composite, and ii) the various average electro-magneto-mechanical fields of the phases
- Ability of the proposed model to predict both macroscopic and average microscopic fields per phase when nonlinear fields take place

Piezoelectric-piezomagnetic behaviour of coated long fiber composites accounting for eigenfields

George Chatzigeorgiou[a,*], Adil Benaarbia[a], Fodil Meraghni[a]

[a]*Arts et Métiers ParisTech, CNRS, Université de Lorraine, LEM3, F-57000, Metz, France*

Abstract

A unified micromechanical approach is proposed to evaluate the electro-magneto-mechanical response of coated long fiber composites with transversely isotropic piezoelectric-piezomagnetic behaviour. The developed framework takes into account the presence of electro-magneto-mechanical eigenfields. The multiscale strategy is based on solving specific boundary value problems in the same spirit as in the Composite Cylinders Assemblage technique. The solution of these problems provides analytical expressions of the dilute electro-magneto-mechanical concentration tensors. With the help of the latter, the mean-field approach of Mori-Tanaka is adapted to identify i) the overall response of the composite, and ii) the various average electro-magneto-mechanical fields generated in the matrix, the fiber and the coating layers for known macroscopic fields. It is found that the novel approach has the same accuracy as existing homogenization techniques in terms of electro-magneto-mechanical properties. The ability of the proposed model to predict both macroscopic and average microscopic fields per phase when eigenfields take place is finally demonstrated.

Keywords: Composite Cylinders Assemblage; Coated long fiber composites; Piezoelectric-piezomagnetic materials, Electro-magneto-inelastic fields;

1. Introduction

Piezoelectric and piezomagnetic materials have received much attention in the last decades and are being increasingly used in various applications such as aerospace, biomedical, vibration

*Corresponding author.

Email addresses: georges.chatzigeorgiou@ensam.eu (George Chatzigeorgiou), adil.benaarbia@ensam.eu (Adil Benaarbia), fodil.meraghni@ensam.eu (Fodil Meraghni)

control and many others. These materials are extensively used as actuators, sensors and transducers. Typically, active actuator materials have the capability to convert electrical and/or magnetic energy into mechanical energy, while sensor materials provide an opposite conversion. To avoid the increased weight of conventional piezoelectric or piezomagnetic materials, these smart materials are generally combined with polymers in the form of composites. Such combination permits to develop new transducers and sensors with high strength, increased thermal conductivity, low thermal expansion and advanced electromechanical behaviour. However, the co-existence of piezoelectic and piezomagnetic coupling effects in such composite materials and the involvement of many constituents-based parameters make the modelling of their multiphysical behaviour complex. From a micromechanics point of view, special techniques are required to investigate the coupling effects and the whole performance of the composite. Such modelling tools hold the key for using these smart composites in many applications in more intelligent ways.

The modelling of the piezoelectric-piezomagnetic composites is still an open topic (e.g., Nan, 1994; Wu and Huang, 2000; Bishay and Atluri, 2016; Ye et al., 2018; Kuo and Hsin, 2018, etc.). Within the last 30 years, significant progress has been made in the development of models that study the combined thermo-electro-magneto-elastic behaviour of composites (Tang and Yu, 2009; Bravo-Castillero et al., 2009; Akbarzadeh and Chen, 2014; Koutsawa, 2015). Most of the existing models in literature were focused on the thermoelastic regime and have paid particular attention to the study of both piezoelectric and piezomagnetic coupling effects. Dunn and Taya (1993) have developed an Eshelby-type approach to investigate the electroelastic behaviour of piezoelectric composite materials by identifying appropriate Eshelby and concentration tensors. This approach has then been extended to consider electro-magneto-elastic responses (Huang and Kuo, 1997; Li and Dunn, 1998; Li, 2000). Huang et al. (1998) have identified electro-magneto-elastic Eshelby tensors for elliptical, rod, penny and ribbon shaped inclusions. Benveniste (1995) has studied the electro-magnetic effect in fibrous composites with piezoelectric and piezomagnetic phases using the composite cylinders assemblage method. Aboudi (2001) has developed a homogenization micromechanical method for the prediction of the effective moduli of coupled electro-magneto-thermo-elastic composites, while Lee et al. (2005) have proposed numerical and Eshelby-based analytical strategies for three phase electro-magneto-elastic composites. Moreover,

the electro-magneto-thermo-elastic composites have extensively been studied using the periodic homogenization theory (Bravo-Castillero et al., 2008, 2009; Challagulla and Georgiades, 2011; Hadjiloizi et al., 2013; Kuo and Peng, 2013). Pakam and Arockiarajan (2014) have developed a micromechanical scheme for studying ferroelectric and magnetostrictive composites reinforced with square cross section fibers and subjected to high electro-magnetic loading conditions. Using Hill's interfacial operators, Dinzart and Sabar (2011) and Koutsawa et al. (2011) have proposed micromechanical models based on Mori-Tanaka and self consistent schemes to investigate the thermo-electro-magneto-elastic behaviour of magneto-piezoelectric composites with multi-coated ellipsoidal particles.

This work aims at developing a unified micromechanical approach in inelasticity to analytically express the electro-magneto-elastic and inelastic concentration tensors and effective material parameters for coated long fiber composites with transversely isotropic piezoelectric-piezomagnetic behaviour. The coating between the matrix and the reinforcement is witnessing strong coupling effects with complex local behaviour. Inelastic deformation mechanisms such as plasticity and/or martensite transformation occur frequently at the coating region and strongly interact with the local damage of the matrix/reinforcement interface (Payandeh et al., 2010, 2012). To reiterate, one of the aims of this work is to develop appropriate tools to assess the electro-magneto-inelastic fields in the matrix, fibers and coating layers. The current work aims at elaborating multiscale approaches to design more accurate damage and failure criteria for piezoelectric-piezomagnetic composites.

A novel approach, adapted to the Mori-Tanaka homogenization scheme, is presented in this manuscript. The approach is based on solving specific boundary value problems, extending the composite cylinders model of Hashin and Rosen (1964) to account for the inelasticity. The latter effort can be considered as a generalization of the Dvorak and Benveniste (1992) methodology, providing analytical expressions of the dilute electro-magneto-mechanical concentration tensors, which can be utilized in classical micromechanical techniques, such as Mori-Tanaka or self consistent methods. The advantage of such information is that it permits to identify not only the overall response of the composite, but also the various average electro-magneto-mechanical fields generated in the matrix, the fiber and the coating layers for known macroscopic electro-magneto-

mechanical conditions.

The effect of eigenfields (inelastic strains, electric or magnetic eigenfields) on the overall response, as well as in the average response of the phases, is important for the study of nonlinear behaviour of composites. Indeed, while in the current manuscript the described boundary value problems are linear, the provided solutions can be seen as the mean to include nonlinear mechanisms per phase. The latter should be described through evolution laws of the nonlinear fields and activation criteria. Via an appropriate incremental, iterative scheme, one can use the linearized micromechanics solution provided here and adapt it to account for the constitutive laws of the phases (see for instance Pettermann et al., 1999 for purely mechanical multiscale analysis).

To fulfill the underlined objectives, a brief description of the Eshelby's problem for coated inhomogeneity with eigenfields at the matrix fibers and coating layers is first presented. The Eshelby problem is then solved by considering special boundary condition problems analogue to those introduced by Hashin and Rosen. Then, numerical computations are conducted and discussed in detail. These computations have permitted to demonstrate the capabilities of the developed micromechanics technique. Several conclusions, drawn from the findings, are finally put forward.

2. Preliminaries

For small deformations and rotations, electrostatic conditions with no electric charge and magnetostatic conditions with no current density, the strain tensor, $\boldsymbol{\varepsilon}$, the electric field vector, $\mathbb{e}$, and the magnetic field vector, $\mathbb{h}$, can be expressed with the help of the displacement vector, $\boldsymbol{u}$, the electric scalar potential, $\mathbb{a}^e$, and the magnetic scalar potential[1], $\mathbb{a}^m$, respectively, through the tensorial relations

$$\boldsymbol{\varepsilon} = \frac{1}{2}\left[\operatorname{grad}\boldsymbol{u} + [\operatorname{grad}\boldsymbol{u}]^T\right], \quad \mathbb{e} = -\operatorname{grad}\mathbb{a}^e \text{ and } \mathbb{h} = -\operatorname{grad}\mathbb{a}^m, \tag{1}$$

[1] In classical magnetomechanics studies, the natural choice is to introduce a vector potential. When dealing with multiscale approaches, the absence of microscopic current density permits an alternative formalism with scalar potential, which simplifies the calculations.

or the vector-type equations

$$\begin{aligned}\boldsymbol{\varepsilon} &= \left[\begin{array}{cccccc} \varepsilon_{11} & \varepsilon_{22} & \varepsilon_{33} & 2\varepsilon_{12} & 2\varepsilon_{13} & 2\varepsilon_{23} \end{array}\right]^T \\ &= \left[\begin{array}{cccccc} \dfrac{\partial u_1}{\partial x_1} & \dfrac{\partial u_2}{\partial x_2} & \dfrac{\partial u_3}{\partial x_3} & \dfrac{\partial u_1}{\partial x_2}+\dfrac{\partial u_2}{\partial x_1} & \dfrac{\partial u_1}{\partial x_3}+\dfrac{\partial u_3}{\partial x_1} & \dfrac{\partial u_2}{\partial x_3}+\dfrac{\partial u_3}{\partial x_2} \end{array}\right]^T, \end{aligned} \tag{2}$$

$$\mathbb{e} = \left[\begin{array}{ccc} \mathbb{e}_1 & \mathbb{e}_2 & \mathbb{e}_3 \end{array}\right]^T = \left[\begin{array}{ccc} -\dfrac{\partial \mathbb{a}^e}{\partial x_1} & -\dfrac{\partial \mathbb{a}^e}{\partial x_2} & -\dfrac{\partial \mathbb{a}^e}{\partial x_3} \end{array}\right]^T, \tag{3}$$

$$\mathbb{h} = \left[\begin{array}{ccc} \mathbb{h}_1 & \mathbb{h}_2 & \mathbb{h}_3 \end{array}\right]^T = \left[\begin{array}{ccc} -\dfrac{\partial \mathbb{a}^m}{\partial x_1} & -\dfrac{\partial \mathbb{a}^m}{\partial x_2} & -\dfrac{\partial \mathbb{a}^m}{\partial x_3} \end{array}\right]^T, \tag{4}$$

where the symbol $[.]^T$ stands for the usual vector/matrix transposes in orthogonal coordinates.

On the other hand, the stress tensor, $\boldsymbol{\sigma}$, the electric displacement, $\mathbb{d}$, and the magnetic induction, $\mathbb{b}$, written in the vector-type forms

$$\begin{aligned}\boldsymbol{\sigma} &= \left[\begin{array}{cccccc} \sigma_{11} & \sigma_{22} & \sigma_{33} & \sigma_{12} & \sigma_{13} & \sigma_{23} \end{array}\right]^T, \\ \mathbb{d} &= \left[\begin{array}{ccc} \mathbb{d}_1 & \mathbb{d}_2 & \mathbb{d}_3 \end{array}\right]^T, \quad \mathbb{b} = \left[\begin{array}{ccc} \mathbb{b}_1 & \mathbb{b}_2 & \mathbb{b}_3 \end{array}\right]^T, \end{aligned} \tag{5}$$

obey the following equilibrium, electrostatic and magnetostatic equations

$$\operatorname{div}\boldsymbol{\sigma} = \mathbf{0}, \quad \operatorname{div}\mathbb{d} = 0 \ \text{ and } \ \operatorname{div}\mathbb{b} = 0, \tag{6}$$

or, in indicial form,

$$\begin{aligned} \partial\sigma_{11}/\partial x_1 + \partial\sigma_{12}/\partial x_2 + \partial\sigma_{13}/\partial x_3 &= 0, \\ \partial\sigma_{12}/\partial x_1 + \partial\sigma_{22}/\partial x_2 + \partial\sigma_{23}/\partial x_3 &= 0, \\ \partial\sigma_{13}/\partial x_1 + \partial\sigma_{23}/\partial x_2 + \partial\sigma_{33}/\partial x_3 &= 0, \\ \partial\mathbb{d}_1/\partial x_1 + \partial\mathbb{d}_2/\partial x_2 + \partial\mathbb{d}_3/\partial x_3 &= 0, \\ \partial\mathbb{b}_1/\partial x_1 + \partial\mathbb{b}_2/\partial x_2 + \partial\mathbb{b}_3/\partial x_3 &= 0. \end{aligned} \tag{7}$$

Besides, a piezo-electro-magnetic, transversely isotropic material with eigenfields obeys the fol-

lowing constitutive laws, written in matrix-type notation[2]

$$\begin{aligned}
\boldsymbol{\sigma} &= \boldsymbol{L}\cdot\left[\boldsymbol{\varepsilon}-\boldsymbol{\varepsilon}^{p}\right]-\boldsymbol{e}\cdot\left[\mathfrak{e}-\mathfrak{e}^{p}\right]-\boldsymbol{f}\cdot\left[\mathbb{h}-\mathbb{h}^{p}\right],\\
\mathfrak{d} &= \boldsymbol{e}^{T}\cdot\left[\boldsymbol{\varepsilon}-\boldsymbol{\varepsilon}^{p}\right]+\boldsymbol{\kappa}^{e}\cdot\left[\mathfrak{e}-\mathfrak{e}^{p}\right]+\boldsymbol{j}\cdot\left[\mathbb{h}-\mathbb{h}^{p}\right],\\
\mathbb{b} &= \boldsymbol{f}^{T}\cdot\left[\boldsymbol{\varepsilon}-\boldsymbol{\varepsilon}^{p}\right]+\boldsymbol{j}^{T}\cdot\left[\mathfrak{e}-\mathfrak{e}^{p}\right]+\boldsymbol{\kappa}^{m}\cdot\left[\mathbb{h}-\mathbb{h}^{p}\right],
\end{aligned} \tag{8}$$

where the index p above a field denotes an eigenfield. Example of eigenfields are those generated by the presence of temperature (e.g. thermal expansion strain, etc.). In addition, $\boldsymbol{L}$, $\boldsymbol{\kappa}^{e}$, $\boldsymbol{\kappa}^{m}$, $\boldsymbol{e}$, $\boldsymbol{f}$, $\boldsymbol{j}$ denote the elasticity, the dielectric properties, the magnetic permeabilities, the coupled electro-mechanical, the coupled magneto-mechanical and the coupled electro-magnetic tensors, respectively. For transversely isotropic behaviour with axis of symmetry parallel to the direction 3, these tensors are expressed in the following matrix-type forms

$$\boldsymbol{L} = \begin{bmatrix}
K^{\mathrm{tr}}+\mu^{\mathrm{tr}} & K^{\mathrm{tr}}-\mu^{\mathrm{tr}} & l & 0 & 0 & 0\\
K^{\mathrm{tr}}-\mu^{\mathrm{tr}} & K^{\mathrm{tr}}+\mu^{\mathrm{tr}} & l & 0 & 0 & 0\\
l & l & n & 0 & 0 & 0\\
0 & 0 & 0 & \mu^{\mathrm{tr}} & 0 & 0\\
0 & 0 & 0 & 0 & \mu^{\mathrm{ax}} & 0\\
0 & 0 & 0 & 0 & 0 & \mu^{\mathrm{ax}}
\end{bmatrix}, \tag{9}$$

$$\boldsymbol{e} = \begin{bmatrix}
0 & 0 & e_{31}\\
0 & 0 & e_{31}\\
0 & 0 & e_{33}\\
0 & 0 & 0\\
e_{15} & 0 & 0\\
0 & e_{15} & 0
\end{bmatrix}, \quad \boldsymbol{f} = \begin{bmatrix}
0 & 0 & f_{31}\\
0 & 0 & f_{31}\\
0 & 0 & f_{33}\\
0 & 0 & 0\\
f_{15} & 0 & 0\\
0 & f_{15} & 0
\end{bmatrix}, \tag{10}$$

[2]The symbol $\cdot$ in the matrix notation denotes the common matrix multiplication. The product between a scalar and a matrix is represented without a symbol.

$$\boldsymbol{\kappa}^e = \begin{bmatrix} \kappa^e_{11} & 0 & 0 \\ 0 & \kappa^e_{11} & 0 \\ 0 & 0 & \kappa^e_{33} \end{bmatrix}, \quad \boldsymbol{\kappa}^m = \begin{bmatrix} \kappa^m_{11} & 0 & 0 \\ 0 & \kappa^m_{11} & 0 \\ 0 & 0 & \kappa^m_{33} \end{bmatrix}, \tag{11}$$

$$\boldsymbol{j} = \begin{bmatrix} j_{11} & 0 & 0 \\ 0 & j_{11} & 0 \\ 0 & 0 & j_{33} \end{bmatrix}. \tag{12}$$

The constants K^{tr}, l, n, μ^{tr}, μ^{ax}, e_{31}, e_{33}, e_{15}, f_{31}, f_{33}, f_{15}, κ^e_{11}, κ^e_{33}, κ^m_{11}, κ^m_{33}, j_{11} and j_{33} are material parameters. Equation (8) can also be written in the following compact form

$$\boldsymbol{\Sigma} = \boldsymbol{\mathcal{L}} \cdot \left[\boldsymbol{E} - \boldsymbol{E}^p \right], \tag{13}$$

where $\boldsymbol{\mathcal{L}}$ is the 12×12 symmetric matrix given as

$$\boldsymbol{\mathcal{L}} = \begin{bmatrix} \boldsymbol{L} & \boldsymbol{e} & \boldsymbol{f} \\ \boldsymbol{e}^T & -\boldsymbol{\kappa}^e & -\boldsymbol{j} \\ \boldsymbol{f}^T & -\boldsymbol{j}^T & -\boldsymbol{\kappa}^m \end{bmatrix}, \tag{14}$$

and $\boldsymbol{\Sigma}$, $\boldsymbol{E}$, $\boldsymbol{E}^p$ the 12×1 vectors defined as

$$\boldsymbol{\Sigma} = \begin{bmatrix} \boldsymbol{\sigma} & \mathbb{d} & \mathbb{b} \end{bmatrix}^T, \quad \boldsymbol{E} = \begin{bmatrix} \boldsymbol{\varepsilon} & -\mathbb{e} & -\mathbb{h} \end{bmatrix}^T, \quad \boldsymbol{E}^p = \begin{bmatrix} \boldsymbol{\varepsilon}^p & -\mathbb{e}^p & -\mathbb{h}^p \end{bmatrix}^T. \tag{15}$$

Finally, the generalized vector

$$\boldsymbol{U} = \begin{bmatrix} u_1 & u_2 & u_3 & \mathbb{a}^e & \mathbb{a}^m \end{bmatrix}^T, \tag{16}$$

is also introduced.

In the sequel, when dealing with various material phases, the following notation is postulated for a quantity a: i) A superscript on the symbol of the form $a^{(q)}$ denotes that the quantity a is spatially dependent. ii) A subscript on the symbol of the form a_q is used for constant or average value of the quantity. The index q can take the values 0, 1 or 2.

3. Coated long fiber composites with eigenfields

Identifying the overall properties of a composite sensitive to electro-magneto-mechanical loading conditions is the task of homogenization strategies and techniques. In this paper, the mean-field approach of the Mori-Tanaka method is followed. This method relies on two aspects:

- solving a basic (Eshelby-type) problem of a coated inhomogeneity embedded in an infinite medium, allowing to compute the so-called "interaction" or "dilute concentration" tensors.
- using this information in the level of the composite for identifying the "concentration" tensors, whose knowledge leads to link the microscopic and macroscopic fields in order to obtain the macroscopic matrix $\overline{\boldsymbol{\mathcal{L}}}$ and the macroscopic eigenfield $\overline{\boldsymbol{E}}^p$ of the overall composite.

3.1. Eshelby's problem for coated inhomogeneity with eigenfields in all phases

Consider a coated cylindrical inhomogeneity, embedded in an infinite medium. The medium, the inhomogeneity and the homothetic coated layer are characterized by constant generalized moduli, $\boldsymbol{\mathcal{L}}_0$, $\boldsymbol{\mathcal{L}}_1$ and $\boldsymbol{\mathcal{L}}_2$, respectively. The inhomogeneity occupies the space Ω_1 with volume V_1, is bounded by the surface $\partial\Omega_1$ and is subjected to the uniform eigenfield $\boldsymbol{E}_1^p$. The coating layer occupies the space Ω_2 with volume V_2, is bounded by the surfaces $\partial\Omega_1$ and $\partial\Omega_2$ and is subjected to the uniform eigenfield $\boldsymbol{E}_2^p$. The medium occupies the space Ω_0, which is extended to infinity (boundary surface $\partial\Omega_\infty$), and is subjected to the uniform eigenstrain $\boldsymbol{E}_0^p$. At far distance, a linear field

$$\boldsymbol{U}_{\text{ext}} = \begin{bmatrix} u_{0_1} \\ u_{0_2} \\ u_{0_3} \\ \mathrm{a}_0^e \\ \mathrm{a}_0^m \end{bmatrix} = \begin{bmatrix} \varepsilon_{11_0} x_1 + \varepsilon_{12_0} x_2 + \varepsilon_{13_0} x_3 \\ \varepsilon_{12_0} x_1 + \varepsilon_{22_0} x_2 + \varepsilon_{23_0} x_3 \\ \varepsilon_{13_0} x_1 + \varepsilon_{23_0} x_2 + \varepsilon_{33_0} x_3 \\ -\mathrm{e}_{1_0} x_1 - \mathrm{e}_{2_0} x_2 - \mathrm{e}_{3_0} x_3 \\ -\mathrm{h}_{1_0} x_1 - \mathrm{h}_{2_0} x_2 - \mathrm{h}_{3_0} x_3 \end{bmatrix}, \tag{17}$$

with ε_{ij_0}, e_{i_0}, h_{i_0} $(i, j = 1, 2, 3)$ constant values, is applied (see Figure 1).

For this problem, which is a generalized version of the famous Eshelby inhomogeneity problem (Eshelby, 1957) accounting for multiphysics phenomena, the constitutive law is position dependent and reads

$$\boldsymbol{\Sigma}(\boldsymbol{x}) = \begin{cases} \boldsymbol{\mathcal{L}}_0 \cdot \left[\boldsymbol{E}(\boldsymbol{x}) - \boldsymbol{E}_0^p\right], & \boldsymbol{x} \in \Omega_0, \\ \boldsymbol{\mathcal{L}}_1 \cdot \left[\boldsymbol{E}(\boldsymbol{x}) - \boldsymbol{E}_1^p\right], & \boldsymbol{x} \in \Omega_1, \\ \boldsymbol{\mathcal{L}}_2 \cdot \left[\boldsymbol{E}(\boldsymbol{x}) - \boldsymbol{E}_2^p\right], & \boldsymbol{x} \in \Omega_2. \end{cases} \tag{18}$$

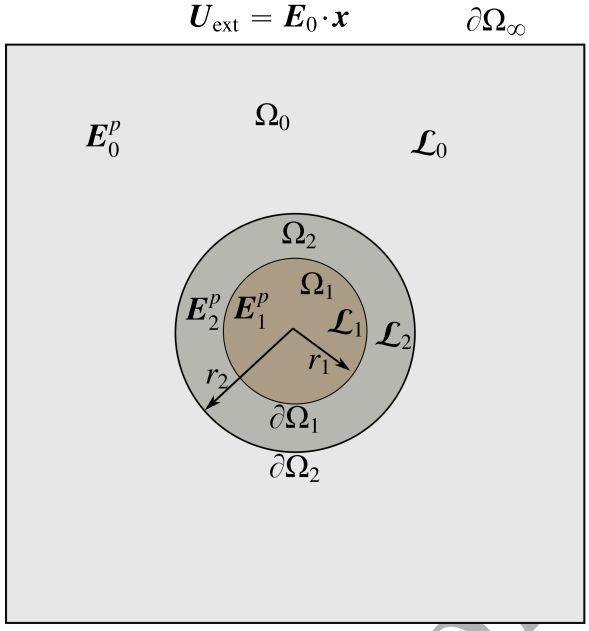

Figure 1: Cross section of coated cylindrical fiber with homothetic topology inside an infinite medium. All phases have homogeneous material properties and are subjected to uniform eigenfields. Moreover, the medium is subjected to linear displacement, electric potential and magnetic potential at far distance.

The boundary conditions correspond to uniform $\boldsymbol{E}_0$ at far distance.

The main goal of this problem is to compute the average fields inside the inhomogeneity and inside the coating layer

$$\boldsymbol{E}_1 = \frac{1}{V_1}\int_{\Omega_1} \boldsymbol{E}(\boldsymbol{x})\mathrm{d}\boldsymbol{x} \quad \text{and} \quad \boldsymbol{E}_2 = \frac{1}{V_2}\int_{\Omega_2} \boldsymbol{E}(\boldsymbol{x})\mathrm{d}\boldsymbol{x}, \tag{19}$$

respectively, when the applied field, $\boldsymbol{E}_0$, at far distance and the eigenfields $\boldsymbol{E}_0^p$, $\boldsymbol{E}_1^p$, $\boldsymbol{E}_2^p$ are known. In other words, the purpose is to evaluate the generalized, 12×12 elastic and inelastic interaction tensors, $\boldsymbol{T}_i$ and $\boldsymbol{T}_{q,i}^p$ for $i = 1, 2$ and $q = 0, 1, 2$, for which the following relations hold

$$\boldsymbol{E}_i \;=\; \boldsymbol{T}_i \cdot \boldsymbol{E}_0 + \sum_{q=0}^{2} \boldsymbol{T}_{q,i}^p \cdot \boldsymbol{E}_q^p. \tag{20}$$

The above expression is a direct extension of the corresponding one in the original Transformation Field Analysis approach of Dvorak and Benveniste (1992). In purely mechanical problems, the first term is the usual elastic interaction tensor of a phase, connecting the total strain in the phase i with the far field applied strain. The sum of the following terms expresses the dependence of the

total strain in the phase i from the inelastic strains of all the phases in the representative volume element.

To assist the computations, the ratio $\phi = V_1/[V_1 + V_2]$ is identified.

3.2. Proposed methodology: analytical solutions in special boundary value problems

The proposed methodology is motivated by the studied boundary value problems by Hashin and Rosen (1964) in their famous composite cylinders assemblage theory. The necessary modifications on these problems, discussed in the sequel, provide the exact solution for the interaction tensors. Similar technique has been utilized in various articles (Benveniste et al., 1989; Chatzigeorgiou et al., 2012; Wang et al., 2016; Chatzigeorgiou and Meraghni, 2019; Chatzigeorgiou et al., 2019) for studying the mechanical and piezoelectric response of long fiber composites.

Before passing to the actual boundary value problems, it is essential to express all the fields and the conservation laws in cylindrical coordinates.

3.2.1. Expressing the Eshelby's inhomogeneity problem in cylindrical coordinates

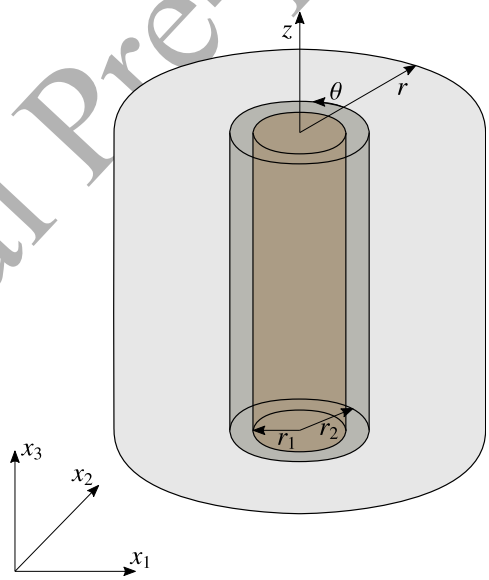

Figure 2: Coated cylindrical fiber with homothetic topology inside an infinite medium, which is represented as a concentric cylinder. All the fields are expressed in cylindrical coordinates.

Inside the representative volume element the various fields generated at every phase q ($q = 0, 1, 2$) depend on the spatial position, i.e

$$\boldsymbol{U}^{(q)}(\boldsymbol{x}), \quad \boldsymbol{E}^{(q)}(\boldsymbol{x}), \quad \boldsymbol{\Sigma}^{(q)}(\boldsymbol{x}), \quad \boldsymbol{E}^{p(q)}(\boldsymbol{x}), \qquad \forall \boldsymbol{x} \in \Omega_q.$$

Due to the geometry of the inhomogeneities, the problem can be transformed in cylindrical coordinates, using a system of concentric cylinders for the inhomogeneity, the coating layer and the infinite matrix (see Figure 2). In cylindrical coordinates, the axes (x, y, z) are transformed to (r, θ, z), according to the relations

$$x_1 = r\cos\theta, \quad x_2 = r\sin\theta, \quad x_3 = z.$$

The vectors and tensors in cylindrical coordinates are noted with an arc above the symbol. Thus, in cylindrical coordinates, the fields are written as

$$\widehat{\boldsymbol{U}}^{(q)}(r,\theta,z), \quad \widehat{\boldsymbol{E}}^{(q)}(r,\theta,z), \quad \widehat{\boldsymbol{\Sigma}}^{(q)}(r,\theta,z), \quad \widehat{\boldsymbol{E}}^{p(q)}(r,\theta,z), \qquad \forall r,\theta,z \in \Omega_q,$$

while the equilibrium, electrostatic and magnetostatic equations are re-expressed as

$$\begin{aligned}
\frac{\partial \widehat{\sigma}_{rr}^{(q)}}{\partial r} + \frac{1}{r}\frac{\partial \widehat{\sigma}_{r\theta}^{(q)}}{\partial \theta} + \frac{\widehat{\sigma}_{rr}^{(q)} - \widehat{\sigma}_{\theta\theta}^{(q)}}{r} + \frac{\partial \widehat{\sigma}_{rz}^{(q)}}{\partial z} &= 0,\\
\frac{\partial \widehat{\sigma}_{r\theta}^{(q)}}{\partial r} + \frac{1}{r}\frac{\partial \widehat{\sigma}_{\theta\theta}^{(q)}}{\partial \theta} + \frac{2\widehat{\sigma}_{r\theta}^{(q)}}{r} + \frac{\partial \widehat{\sigma}_{\theta z}^{(q)}}{\partial z} &= 0,\\
\frac{\partial \widehat{\sigma}_{rz}^{(q)}}{\partial r} + \frac{1}{r}\frac{\partial \widehat{\sigma}_{\theta z}^{(q)}}{\partial \theta} + \frac{\widehat{\sigma}_{rz}^{(q)}}{r} + \frac{\partial \widehat{\sigma}_{zz}^{(q)}}{\partial z} &= 0,\\
\frac{\partial \widehat{\mathbb{d}}_{r}^{(q)}}{\partial r} + \frac{1}{r}\frac{\partial \widehat{\mathbb{d}}_{\theta}^{(q)}}{\partial \theta} + \frac{\widehat{\mathbb{d}}_{r}^{(q)}}{r} + \frac{\partial \widehat{\mathbb{d}}_{z}^{(q)}}{\partial z} &= 0,\\
\frac{\partial \widehat{\mathbb{b}}_{r}^{(q)}}{\partial r} + \frac{1}{r}\frac{\partial \widehat{\mathbb{b}}_{\theta}^{(q)}}{\partial \theta} + \frac{\widehat{\mathbb{b}}_{r}^{(q)}}{r} + \frac{\partial \widehat{\mathbb{b}}_{z}^{(q)}}{\partial z} &= 0.
\end{aligned} \tag{21}$$

In addition, the strain, electric and magnetic field components in each phase are given using the following expressions

$$\begin{aligned}
\widehat{\boldsymbol{\varepsilon}}^{(q)} &= \left[\begin{array}{cccccc} \hat{\varepsilon}_{rr}^{(q)} & \hat{\varepsilon}_{\theta\theta}^{(q)} & \hat{\varepsilon}_{zz}^{(q)} & 2\hat{\varepsilon}_{r\theta}^{(q)} & 2\hat{\varepsilon}_{rz}^{(q)} & 2\hat{\varepsilon}_{\theta z}^{(q)} \end{array}\right]^T\\
&= \left[\begin{array}{ccc} \dfrac{\partial \hat{u}_r^{(q)}}{\partial r} & \dfrac{1}{r}\dfrac{\partial \hat{u}_\theta^{(q)}}{\partial \theta} + \dfrac{\hat{u}_r^{(q)}}{r} & \dfrac{\partial \hat{u}_z^{(q)}}{\partial z} \\ \dfrac{\partial \hat{u}_\theta^{(q)}}{\partial r} + \dfrac{1}{r}\dfrac{\partial \hat{u}_r^{(q)}}{\partial \theta} - \dfrac{\hat{u}_\theta^{(q)}}{r} & \dfrac{\partial \hat{u}_z^{(q)}}{\partial r} + \dfrac{\partial \hat{u}_r^{(q)}}{\partial z} & \dfrac{1}{r}\dfrac{\partial \hat{u}_z^{(q)}}{\partial \theta} + \dfrac{\partial \hat{u}_\theta^{(q)}}{\partial z} \end{array}\right]^T,
\end{aligned} \tag{22}$$

$$\widehat{\mathbb{e}}^{(q)} = \begin{bmatrix} \widehat{\mathbb{e}}_r^{(q)} & \widehat{\mathbb{e}}_\theta^{(q)} & \widehat{\mathbb{e}}_z^{(q)} \end{bmatrix}^T = \begin{bmatrix} -\dfrac{\partial \mathbb{a}^{e(q)}}{\partial r} & -\dfrac{1}{r}\dfrac{\partial \mathbb{a}^{e(q)}}{\partial \theta} & -\dfrac{\partial \mathbb{a}^{e(q)}}{\partial z} \end{bmatrix}^T, \tag{23}$$

$$\widehat{\mathbb{h}}^{(q)} = \begin{bmatrix} \widehat{\mathbb{h}}_r^{(q)} & \widehat{\mathbb{h}}_\theta^{(q)} & \widehat{\mathbb{h}}_z^{(q)} \end{bmatrix}^T = \begin{bmatrix} -\dfrac{\partial \mathbb{a}^{m(q)}}{\partial r} & -\dfrac{1}{r}\dfrac{\partial \mathbb{a}^{m(q)}}{\partial \theta} & -\dfrac{\partial \mathbb{a}^{m(q)}}{\partial z} \end{bmatrix}^T. \tag{24}$$

The inhomogeneity is considered to have radius r equal to r_1 and the coating layer has external radius r_2 (see Figure 1). Using the radii of the concentric cylinders, one obtains $\phi = r_1^2/r_2^2$.

The continuity conditions between i) the inhomogeneity and the coating layer, and ii) the coating and the matrix are expressed through the relations

$$\begin{aligned}
\hat{u}_s^{(1)}(r_1,\theta,z) &= \hat{u}_s^{(2)}(r_1,\theta,z), \quad s = r,\theta \text{ or } z,\\
\hat{u}_s^{(2)}(r_2,\theta,z) &= \hat{u}_s^{(0)}(r_2,\theta,z), \quad s = r,\theta \text{ or } z,\\
\mathbb{a}^{s(1)}(r_1,\theta,z) &= \mathbb{a}^{s(2)}(r_1,\theta,z), \quad s = e \text{ or } m,\\
\mathbb{a}^{s(2)}(r_2,\theta,z) &= \mathbb{a}^{s(0)}(r_2,\theta,z), \quad s = e \text{ or } m,
\end{aligned} \tag{25}$$

and

$$\begin{aligned}
\widehat{\sigma}_S^{(1)}(r_1,\theta,z) &= \widehat{\sigma}_S^{(2)}(r_1,\theta,z), \quad S = rr, r\theta \text{ or } rz,\\
\widehat{\sigma}_S^{(2)}(r_2,\theta,z) &= \widehat{\sigma}_S^{(0)}(r_2,\theta,z), \quad S = rr, r\theta \text{ or } rz,\\
\widehat{\mathbb{d}}_r^{(1)}(r_1,\theta,z) &= \widehat{\mathbb{d}}_r^{(2)}(r_1,\theta,z),\\
\widehat{\mathbb{d}}_r^{(2)}(r_2,\theta,z) &= \widehat{\mathbb{d}}_r^{(0)}(r_2,\theta,z),\\
\widehat{\mathbb{b}}_r^{(1)}(r_1,\theta,z) &= \widehat{\mathbb{b}}_r^{(2)}(r_1,\theta,z),\\
\widehat{\mathbb{b}}_r^{(2)}(r_2,\theta,z) &= \widehat{\mathbb{b}}_r^{(0)}(r_2,\theta,z).
\end{aligned} \tag{26}$$

Due to the transverse isotropy of all phases, the generalized modulus, $\boldsymbol{\mathcal{L}}$, retains the same form in cylindrical coordinates.

In the following subsections, the boundary value problems are presented and the analytical form of the solution (in terms of the generalized vector $\widehat{\boldsymbol{U}}^{(q)}$) is given.

3.2.2. Analytical boundary value problems

The four boundary value problems which allow to compute the interaction tensors are the following:

- *Axial shear / in-plane electric and magnetic field*

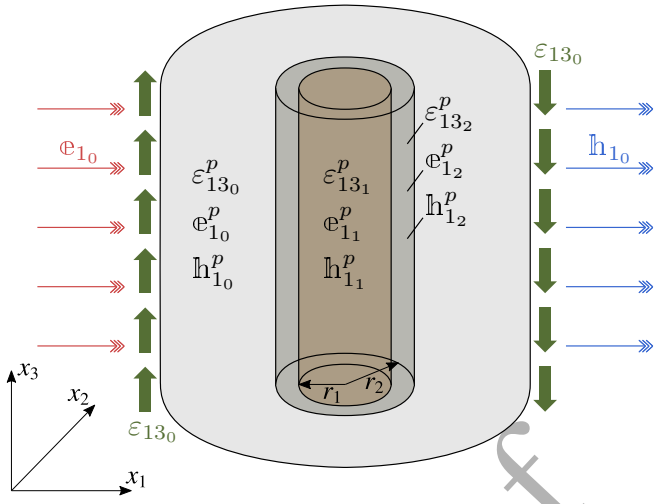

Figure 3: Boundary value problem for axial shear / in-plane electric and magnetic field conditions.

Displacement, electric and magnetic potential boundary conditions at far field (when r_{ext} tends to infinity) are expressed using the following formulas

$$\begin{aligned} \hat{u}_{r\ \text{ext}} &= \hat{u}_{\theta\ \text{ext}} = 0, \\ \hat{u}_{z\ \text{ext}} &= \beta r_{\text{ext}} \cos\theta, \\ \mathfrak{a}^e_{\text{ext}} &= -\beta^e r_{\text{ext}} \cos\theta, \\ \mathfrak{a}^m_{\text{ext}} &= -\beta^m r_{\text{ext}} \cos\theta, \end{aligned} \tag{27}$$

where β, β^e and β^m are considered known. In addition, all phases are subjected to the following eigenfields

$$\begin{aligned} \hat{\boldsymbol{\varepsilon}}^{p(q)} &= s_q \begin{bmatrix} 0 & 0 & 0 & 0 & \cos\theta & -\sin\theta \end{bmatrix}^T, \\ \hat{\mathfrak{e}}^{p(q)} &= s^e_q \begin{bmatrix} \cos\theta & -\sin\theta & 0 \end{bmatrix}^T, \\ \hat{\mathbb{h}}^{p(q)} &= s^m_q \begin{bmatrix} \cos\theta & -\sin\theta & 0 \end{bmatrix}^T, \end{aligned} \tag{28}$$

for $q = 0, 1, 2$ and the values of s_q, s^e_q and s^m_q being known. The latter expressions correspond to uniform shear strain on the plane $x_1 - x_3$ and uniform electric and magnetic field in the

x_1 direction (see Figure 3). The analytical solution for the displacement field, the electric potential and the magnetic potential at every r, θ and z takes the form

$$\begin{aligned}
\hat{u}_r^{(q)} &= \hat{u}_\theta^{(q)} = 0, \\
\hat{u}_z^{(q)} &= r\sum_{i=1}^{2} \Xi_{q,i} \left[\frac{r}{r_1}\right]^{\xi_i - 1} \cos\theta, \\
\mathbb{a}^{e(q)} &= -r\sum_{i=1}^{2} \Xi^e_{q,i} \left[\frac{r}{r_1}\right]^{\xi_i - 1} \cos\theta, \\
\mathbb{a}^{m(q)} &= -r\sum_{i=1}^{2} \Xi^m_{q,i} \left[\frac{r}{r_1}\right]^{\xi_i - 1} \cos\theta,
\end{aligned} \tag{29}$$

with $\xi_1 = 1$ and $\xi_2 = -1$. The unknown coefficients $\Xi_{q,i}$, $\Xi^e_{q,i}$ and $\Xi^m_{q,i}$ are determined from the boundary conditions, the interface relations (25), (26) and the condition that the displacements, the magnetic potential and the electric potential are finite at $r = 0$.

- *Transverse shear strain*

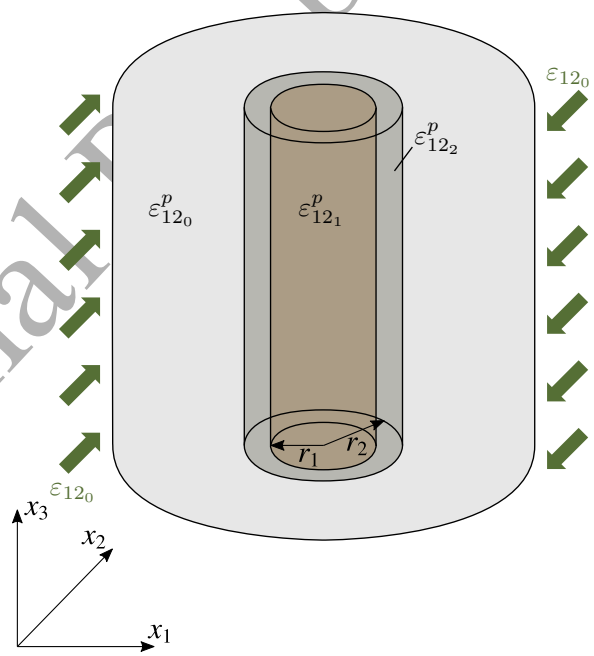

Figure 4: Boundary value problem for transverse shear strain conditions.

Displacement boundary conditions at far field (when r_{ext} tends to infinity) are expressed

using the following equations

$$\begin{aligned} \hat{u}_{r\ \mathrm{ext}} &= \gamma r_{\mathrm{ext}} \sin 2\theta, \\ \hat{u}_{\theta\ \mathrm{ext}} &= \gamma r_{\mathrm{ext}} \cos 2\theta, \\ \hat{u}_{z\ \mathrm{ext}} &= 0, \end{aligned} \tag{30}$$

where γ is known. All phases are also subjected to the eigenstrains

$$\hat{\boldsymbol{\varepsilon}}^{p(q)} = 2s_q \left[\begin{array}{cccccc} \frac{1}{2}\sin 2\theta & -\frac{1}{2}\sin 2\theta & 0 & \cos 2\theta & 0 & 0 \end{array} \right]^T, \tag{31}$$

for $q = 0, 1, 2$ and the value of s_q being known. The latter expression corresponds to uniform shear strain on the plane $x_1 - x_2$ (see Figure 4). The analytical solution for the displacement field at every r, θ and z takes the following form

$$\begin{aligned} \hat{u}_r^{(q)} &= r \sum_{i=1}^{4} \Xi_{q,i} \psi_{q,i} \left[\frac{r}{r_1} \right]^{\xi_i - 1} \sin 2\theta, \\ \hat{u}_\theta^{(q)} &= r \sum_{i=1}^{4} \Xi_{q,i} \left[\frac{r}{r_1} \right]^{\xi_i - 1} \cos 2\theta, \\ \hat{u}_z^{(q)} &= 0, \end{aligned} \tag{32}$$

with

$$\begin{aligned} \xi_1 &= 3, & \psi_{q,1} &= \frac{K_q - \mu_q}{2K_q + \mu_q}, \\ \xi_2 &= 1, & \psi_{q,2} &= 1, \\ \xi_3 &= -3, & \psi_{q,3} &= -1, \\ \xi_4 &= -1, & \psi_{q,4} &= \frac{K_q + \mu_q}{\mu_q}. \end{aligned} \tag{33}$$

In such loading case, the unknown coefficients $\Xi_{q,i}$ are determined from the boundary conditions, the interface relations (25), (26) and the condition that the displacements are finite at $r = 0$.

- *Plane strain / axial electric and magnetic field*

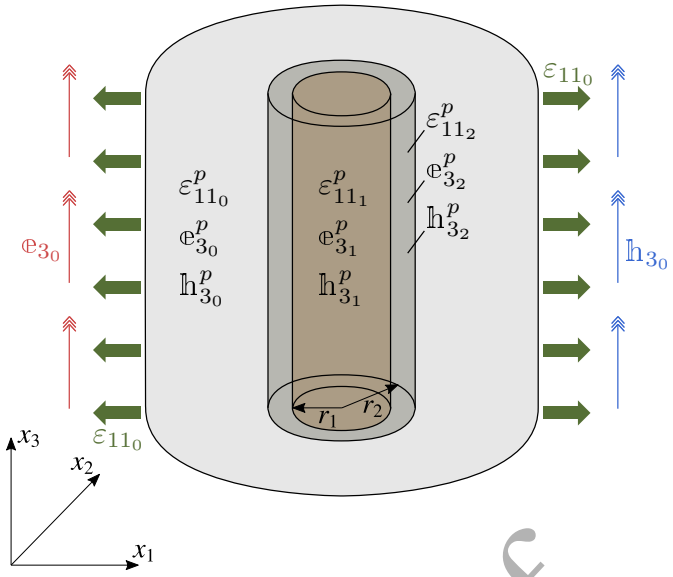

Figure 5: Boundary value plane strain / axial electric and magnetic field conditions. Case of uniaxial strain in the x_1 direction.

Displacement, electric and magnetic potential boundary conditions at far field (when r_{ext} tends to infinity) are expressed as follows

$$\begin{aligned}
\hat{u}_{r\,\text{ext}} &= \beta r_{\text{ext}} + \gamma r_{\text{ext}} \cos 2\theta, \\
\hat{u}_{\theta\,\text{ext}} &= -\gamma r_{\text{ext}} \sin 2\theta, \\
\hat{u}_{z\,\text{ext}} &= 0, \\
\mathfrak{a}^e_{\text{ext}} &= -\beta^e z, \\
\mathfrak{a}^m_{\text{ext}} &= -\beta^m z,
\end{aligned} \tag{34}$$

where β, γ, β^e and β^m are assumed known. All phases are subjected to the eigenfields

$$\begin{aligned}
\widehat{\boldsymbol{\varepsilon}}^{p(q)} &= s_{q,\beta} \begin{bmatrix} 1 & 1 & 0 & 0 & 0 & 0 \end{bmatrix}^T \\
&\quad + 2 s_{q,\gamma} \begin{bmatrix} \frac{1}{2}\cos 2\theta & -\frac{1}{2}\cos 2\theta & 0 & -\sin 2\theta & 0 & 0 \end{bmatrix}^T, \\
\widehat{\mathfrak{e}}^{p(q)} &= s^e_q \begin{bmatrix} 0 & 0 & 1 \end{bmatrix}^T, \\
\widehat{\mathbb{h}}^{p(q)} &= s^m_q \begin{bmatrix} 0 & 0 & 1 \end{bmatrix}^T,
\end{aligned} \tag{35}$$

where the values of $s_{q,\beta}$, $s_{q,\gamma}$, s^e_q and s^m_q are known for $q = 0, 1, 2$. The latter expressions

correspond to uniform biaxial strain state with normal components on the x_1 and x_2 directions, and uniform electric and magnetic fields in the x_3 direction. Two special cases are considered here:

- uniform strain at the x_1 direction, which is obtained by setting $\gamma = \beta$ and $s_{q,\gamma} = s_{q,\beta}$ (see Figure 5),
- uniform strain at the x_2 direction, which is obtained by setting $\gamma = -\beta$ and $s_{q,\gamma} = -s_{q,\beta}$.

The analytical solution for the displacement field, the electric potential and the magnetic potential at every r, θ and z takes the following form

$$\begin{aligned}
\hat{u}_r^{(q)} &= r\sum_{i=1}^{4}\Xi_{q,i}\psi_{q,i}\left[\frac{r}{r_1}\right]^{\xi_i-1}\cos 2\theta + r\sum_{i=1}^{2}Z_{q,i}\left[\frac{r}{r_1}\right]^{\zeta_i-1},\\
\hat{u}_\theta^{(q)} &= -r\sum_{i=1}^{4}\Xi_{q,i}\left[\frac{r}{r_1}\right]^{\xi_i-1}\sin 2\theta,\\
\hat{u}_z^{(q)} &= 0,\\
\mathbb{a}^{e(q)} &= -\beta^e z,\\
\mathbb{a}^{m(q)} &= -\beta^m z.
\end{aligned} \tag{36}$$

In the above expressions, $\zeta_1 = 1$ and $\zeta_2 = -1$, while $\psi_{q,i}$ and ξ_i for $i = 1, 2, 3, 4$ are given by the relations described in the previous boundary value problem. Moreover, the unknown coefficients $\Xi_{q,i}$, $Z_{q,i}$ are determined from the boundary conditions, the interface relations (25), (26) and the condition that the displacements are finite at $r = 0$.

- *Hydrostatic strain / axial inelastic strain*

Displacement boundary conditions at far field correspond to hydrostatic strain where

$$\hat{u}_{r\,\text{ext}} = \beta r_{\text{ext}}, \quad \hat{u}_{\theta\,\text{ext}} = 0 \quad \text{and} \quad \hat{u}_{z\,\text{ext}} = \beta z_{\text{ext}}. \tag{37}$$

All phases are subjected to the eigenstrains

$$\hat{\boldsymbol{\varepsilon}}^{p(q)} = s_q \begin{bmatrix} 0 & 0 & 1 & 0 & 0 & 0 \end{bmatrix}^T, \tag{38}$$

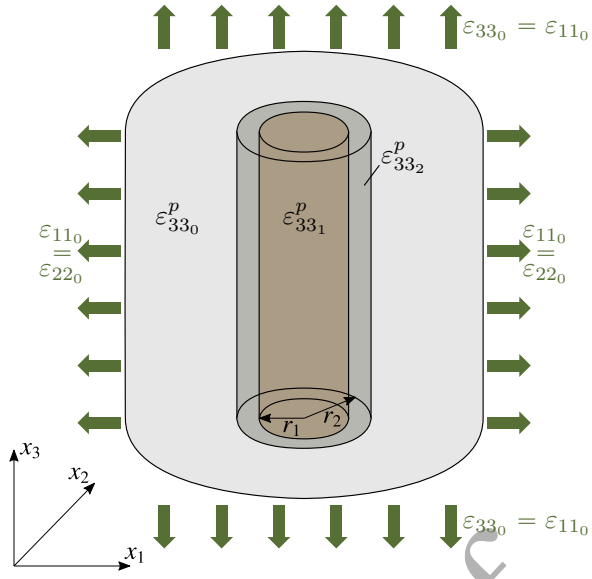

Figure 6: Boundary value problem for hydrostatic strain / axial inelastic strain conditions.

for $q = 0, 1, 2$ and the value of s_q being known. The latter expression corresponds to uniform inelastic strain in the x_3 direction (see Figure 6). The analytical solution for the displacement field at every r, θ and z takes the following form

$$\hat{u}_r^{(q)} = r \sum_{i=1}^{2} Z_{q,i} \left[\frac{r}{r_1}\right]^{\zeta_i - 1}, \quad \hat{u}_\theta^{(q)} = 0 \quad \text{and} \quad \hat{u}_z^{(q)} = \beta z, \tag{39}$$

with $\zeta_1 = 1$ and $\zeta_2 = -1$. The unknown coefficients $Z_{q,i}$ are determined from the boundary conditions, the interface relations (25), (26) and the condition that the displacements are finite at $r = 0$.

3.2.3. *Computing the interaction tensors*

Solving the previously described boundary value problems, the fields $\widehat{\boldsymbol{E}}^{(q)}$ can be computed in both the fiber and its coating. Consequently, the average values $\boldsymbol{E}_1$ and $\boldsymbol{E}_2$, expressed in Cartesian coordinates, can be evaluated analytically with the help of the expressions (19). In these studies, the values of β, γ, β^e, β^m, s_q, $s_{q,\beta}$, $s_{q,\gamma}$, s_q^e and s_q^m can be chosen properly in order to "construct" the interaction tensors (for instance, setting one equal to 1 and zero to the rest). The four discussed boundary value problems are sufficient for identifying all the terms of $\boldsymbol{T}_i$ and $\boldsymbol{T}_{q,i}^p$. The computations are lengthy and are omitted in the current manuscript. Similar computational procedure is

described in Chatzigeorgiou and Meraghni (2019); Chatzigeorgiou et al. (2019).

It is important to note that the general forms of the elastic and inelastic interaction tensors in all phases are given by the expressions

$$\boldsymbol{T} = \begin{bmatrix} \boldsymbol{T}^{00} & \boldsymbol{T}^{0e} & \boldsymbol{T}^{0m} \\ \boldsymbol{T}^{e0} & \boldsymbol{T}^{ee} & \boldsymbol{T}^{em} \\ \boldsymbol{T}^{m0} & \boldsymbol{T}^{me} & \boldsymbol{T}^{mm} \end{bmatrix}, \quad \boldsymbol{T}^{p} = \begin{bmatrix} \boldsymbol{T}^{p00} & \boldsymbol{T}^{p0e} & \boldsymbol{T}^{p0m} \\ \boldsymbol{T}^{pe0} & \boldsymbol{T}^{pee} & \boldsymbol{T}^{pem} \\ \boldsymbol{T}^{pm0} & \boldsymbol{T}^{pme} & \boldsymbol{T}^{pmm} \end{bmatrix}, \tag{40}$$

where the various submatrices are written as

$$\boldsymbol{T}^{00} = \begin{bmatrix} \frac{1}{2}\left[[T_{xx}]_{\text{mec}} + [T_{xy}]_{\text{mec}}\right] & \frac{1}{2}\left[[T_{xx}]_{\text{mec}} - [T_{xy}]_{\text{mec}}\right] & [T_{zz}]_{\text{mec}} - [T_{xx}]_{\text{mec}} & 0 & 0 & 0 \\ \frac{1}{2}\left[[T_{xx}]_{\text{mec}} - [T_{xy}]_{\text{mec}}\right] & \frac{1}{2}\left[[T_{xx}]_{\text{mec}} + [T_{xy}]_{\text{mec}}\right] & [T_{zz}]_{\text{mec}} - [T_{xx}]_{\text{mec}} & 0 & 0 & 0 \\ 0 & 0 & 1 & 0 & 0 & 0 \\ 0 & 0 & 0 & [T_{xy}]_{\text{mec}} & 0 & 0 \\ 0 & 0 & 0 & 0 & [T_{xz}]_{\text{mec}} & 0 \\ 0 & 0 & 0 & 0 & 0 & [T_{xz}]_{\text{mec}} \end{bmatrix}, \tag{41}$$

$$\boldsymbol{T}^{p00} = \begin{bmatrix} \frac{1}{2}\left[[T^{p}_{xx}]_{\text{mec}} + [T^{p}_{xy}]_{\text{mec}}\right] & \frac{1}{2}\left[[T^{p}_{xx}]_{\text{mec}} - [T^{p}_{xy}]_{\text{mec}}\right] & [T^{p}_{zz}]_{\text{mec}} - [T^{p}_{xx}]_{\text{mec}} & 0 & 0 & 0 \\ \frac{1}{2}\left[[T^{p}_{xx}]_{\text{mec}} - [T^{p}_{xy}]_{\text{mec}}\right] & \frac{1}{2}\left[[T^{p}_{xx}]_{\text{mec}} + [T^{p}_{xy}]_{\text{mec}}\right] & [T^{p}_{zz}]_{\text{mec}} - [T^{p}_{xx}]_{\text{mec}} & 0 & 0 & 0 \\ 0 & 0 & 0 & 0 & 0 & 0 \\ 0 & 0 & 0 & [T^{p}_{xy}]_{\text{mec}} & 0 & 0 \\ 0 & 0 & 0 & 0 & [T^{p}_{xz}]_{\text{mec}} & 0 \\ 0 & 0 & 0 & 0 & 0 & [T^{p}_{xz}]_{\text{mec}} \end{bmatrix}, \tag{42}$$

$$\boldsymbol{T}^{e0} = \begin{bmatrix} 0 & 0 & 0 & 0 & \left[T^{e}_{xz}\right]_{\text{mec}} & 0 \\ 0 & 0 & 0 & 0 & 0 & \left[T^{e}_{xz}\right]_{\text{mec}} \\ 0 & 0 & 0 & 0 & 0 & 0 \end{bmatrix}, \tag{43}$$

$$\boldsymbol{T}^{pe0} = \begin{bmatrix} 0 & 0 & 0 & 0 & [T_{xz}^{pe}]_{\text{mec}} & 0 \\ 0 & 0 & 0 & 0 & 0 & [T_{xz}^{pe}]_{\text{mec}} \\ 0 & 0 & 0 & 0 & 0 & 0 \end{bmatrix}, \tag{44}$$

$$\boldsymbol{T}^{m0} = \begin{bmatrix} 0 & 0 & 0 & 0 & \left[T_{xz}^{m}\right]_{\text{mec}} & 0 \\ 0 & 0 & 0 & 0 & 0 & \left[T_{xz}^{m}\right]_{\text{mec}} \\ 0 & 0 & 0 & 0 & 0 & 0 \end{bmatrix}, \tag{45}$$

$$\boldsymbol{T}^{pm0} = \begin{bmatrix} 0 & 0 & 0 & 0 & [T_{xz}^{pm}]_{\text{mec}} & 0 \\ 0 & 0 & 0 & 0 & 0 & [T_{xz}^{pm}]_{\text{mec}} \\ 0 & 0 & 0 & 0 & 0 & 0 \end{bmatrix}, \tag{46}$$

$$\boldsymbol{T}^{0e} = \begin{bmatrix} 0 & 0 & [T_{xx}]_{\text{elc}} \\ 0 & 0 & [T_{xx}]_{\text{elc}} \\ 0 & 0 & 0 \\ 0 & 0 & 0 \\ [T_{xz}]_{\text{elc}} & 0 & 0 \\ 0 & [T_{xz}]_{\text{elc}} & 0 \end{bmatrix}, \quad \boldsymbol{T}^{p0e} = \begin{bmatrix} 0 & 0 & [T_{xx}^{p}]_{\text{elc}} \\ 0 & 0 & [T_{xx}^{p}]_{\text{elc}} \\ 0 & 0 & 0 \\ 0 & 0 & 0 \\ [T_{xz}^{p}]_{\text{elc}} & 0 & 0 \\ 0 & [T_{xz}^{p}]_{\text{elc}} & 0 \end{bmatrix}, \tag{47}$$

$$\boldsymbol{T}^{0m} = \begin{bmatrix} 0 & 0 & [T_{xx}]_{\text{mag}} \\ 0 & 0 & [T_{xx}]_{\text{mag}} \\ 0 & 0 & 0 \\ 0 & 0 & 0 \\ [T_{xz}]_{\text{mag}} & 0 & 0 \\ 0 & [T_{xz}]_{\text{mag}} & 0 \end{bmatrix}, \quad \boldsymbol{T}^{p0m} = \begin{bmatrix} 0 & 0 & [T^p_{xx}]_{\text{mag}} \\ 0 & 0 & [T^p_{xx}]_{\text{mag}} \\ 0 & 0 & 0 \\ 0 & 0 & 0 \\ [T^p_{xz}]_{\text{mag}} & 0 & 0 \\ 0 & [T^p_{xz}]_{\text{mag}} & 0 \end{bmatrix}, \tag{48}$$

$$\boldsymbol{T}^{ee} = \begin{bmatrix} [T^e_{xz}]_{\text{elc}} & 0 & 0 \\ 0 & [T^e_{xz}]_{\text{elc}} & 0 \\ 0 & 0 & 1 \end{bmatrix}, \quad \boldsymbol{T}^{pee} = \begin{bmatrix} [T^{pe}_{xz}]_{\text{elc}} & 0 & 0 \\ 0 & [T^{pe}_{xz}]_{\text{elc}} & 0 \\ 0 & 0 & 0 \end{bmatrix}, \tag{49}$$

$$\boldsymbol{T}^{mm} = \begin{bmatrix} [T^m_{xz}]_{\text{mag}} & 0 & 0 \\ 0 & [T^m_{xz}]_{\text{mag}} & 0 \\ 0 & 0 & 1 \end{bmatrix}, \quad \boldsymbol{T}^{pmm} = \begin{bmatrix} [T^{pm}_{xz}]_{\text{mag}} & 0 & 0 \\ 0 & [T^{pm}_{xz}]_{\text{mag}} & 0 \\ 0 & 0 & 0 \end{bmatrix}, \tag{50}$$

$$\boldsymbol{T}^{me} = \begin{bmatrix} [T^m_{xz}]_{\text{elc}} & 0 & 0 \\ 0 & [T^m_{xz}]_{\text{elc}} & 0 \\ 0 & 0 & 0 \end{bmatrix}, \quad \boldsymbol{T}^{pme} = \begin{bmatrix} [T^{pm}_{xz}]_{\text{elc}} & 0 & 0 \\ 0 & [T^{pm}_{xz}]_{\text{elc}} & 0 \\ 0 & 0 & 0 \end{bmatrix}, \tag{51}$$

$$\boldsymbol{T}^{em} = \begin{bmatrix} [T^e_{xz}]_{\text{mag}} & 0 & 0 \\ 0 & [T^e_{xz}]_{\text{mag}} & 0 \\ 0 & 0 & 0 \end{bmatrix}, \quad \boldsymbol{T}^{pem} = \begin{bmatrix} [T^{pe}_{xz}]_{\text{mag}} & 0 & 0 \\ 0 & [T^{pe}_{xz}]_{\text{mag}} & 0 \\ 0 & 0 & 0 \end{bmatrix}. \tag{52}$$

In the above formulas, the symbols $[\{\bullet\}]_{\text{mec}}$, $[\{\bullet\}]_{\text{elc}}$ and $[\{\bullet\}]_{\text{mag}}$ denote quantities that are activated by the presence of strains, electric fields and magnetic fields, respectively. Appendix A presents the computational details for obtaining the various T terms.

3.3. Alternative approach: Hill's interfacial operators

The solution to the original problem proposed by Eshelby (1957) is valid for uncoated inhomogeneities of ellipsoidal shape inside a matrix material. In the case of coated inhomogeneity, the Eshelby approach provides information for the average strain inside the inhomogeneity/coating system. To identify the strains at each phase, one can use the concept of the interfacial operators (Walpole, 1978; Hill, 1983). This technique has been widely utilized in the literature for composites with mechanical (Cherkaoui et al., 1995; Berbenni and Cherkaoui, 2010; Chatzigeorgiou and Meraghni, 2019), piezoelectric (Chatzigeorgiou et al., 2019), thermo-piezoelectric (Koutsawa et al., 2010), piezoelectric-piezomagnetic (Dinzart and Sabar, 2011), and thermo-piezoelectric-piezomagnetic (Koutsawa et al., 2011) behaviour.

The computational steps for obtaining the elastic and interaction tensors for a composite with pure mechanical behaviour have been described in detail in Chatzigeorgiou and Meraghni (2019). For a piezoelectric-piezomagnetic composite the procedure is similar, with the only difference that the fields have the extended form presented in section 2. It is important to point out that the use of Hill's interfacial operators implies implicitly the hypothesis that in the Eshelby problem the total fields inside the inhomogeneity are uniform. As has been illustrated in Chatzigeorgiou and Meraghni (2019), under transverse shear conditions this hypothesis is violated in long fiber composites and thus can provide inaccurate results in certain cases.

3.4. Mori-Tanaka approach

Once the tensors $\boldsymbol{T}_i$ and $\boldsymbol{T}^p_{q,i}$ are identified with one of the two approaches discussed previously, one can pass to the next step and consider the composite.

A direct approach, like for instance the generalized self consistent composite cylinders method (Christensen, 1979), is applicable for the problem under investigation. It provides the local distribution of the fields in the representative volume element, but it is quite limited, since it is designed exclusively for unidirectional fiber composites with random distribution of the fibers. The current work considers the Mori-Tanaka method for identifying the macroscopic response of the composite. A mean-field approach is more flexible in terms of microstructural characteristics; it can account for non-uniform distributions of the fibers, or the presence of different types of reinforce-

ment. The restriction of the proposed methodology is that it estimates only average fields per material phase and not their actual spatial distribution, which is the case for full field approaches.

A unidirectional coated fiber composite consists of a matrix phase in which coated fibers are distributed randomly (see Figure 7). In this three-phase composite, the volume fractions of the matrix, the fibers and their coating are denoted as c_q, $q = 0, 1, 2$. Using the ratio, ϕ, the following relations can be given

$$c_2 = -c_1 + \frac{c_1}{\phi} \quad \text{and} \quad c_0 = 1 - \frac{c_1}{\phi}. \tag{53}$$

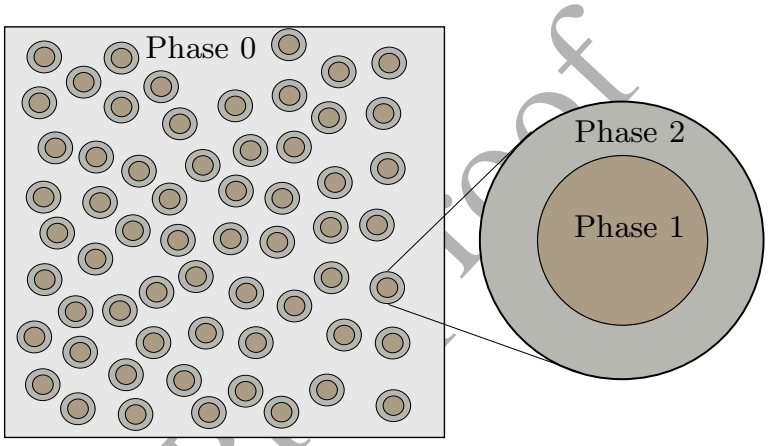

Figure 7: Cross section of unidirectional fiber composite. The fibers are coated and all phases exhibit piezoelectric-piezomagnetic behaviour.

According to the basic principle of all multiscale methods, the macroscopic fields at a macroscopic point are equal to the average of the corresponding microscopic fields over the representative volume element linked with the specific macroscopic point. In the composite considered here, the macroscopic fields, $\overline{\boldsymbol{E}}$ and $\overline{\boldsymbol{\Sigma}}$, are given by

$$\begin{aligned} \overline{\boldsymbol{E}} &= c_0\boldsymbol{E}_0 + c_1\boldsymbol{E}_1 + c_2\boldsymbol{E}_2, \\ \overline{\boldsymbol{\Sigma}} &= c_0\boldsymbol{\Sigma}_0 + c_1\boldsymbol{\Sigma}_1 + c_2\boldsymbol{\Sigma}_2. \end{aligned} \tag{54}$$

Moreover, the constitutive law for each phase can be written in its average form

$$\boldsymbol{\Sigma}_r = \boldsymbol{\mathcal{L}}_r \cdot [\boldsymbol{E}_r - \boldsymbol{E}_r^p], \quad r = 0, 1, 2. \tag{55}$$

In the Mori-Tanaka method, the far field, $\boldsymbol{E}_0$, and the eigenfield, $\boldsymbol{E}_0^p$, of the expressions (20) correspond to the average field and the average eigenfield of the matrix phase of the composite. Combining (20) and $(54)_1$, and after some algebra, the following relations are derived for $r = 0, 1, 2$

$$\boldsymbol{E}_r = \boldsymbol{A}_r \cdot \overline{\boldsymbol{E}} + \sum_{q=0}^{2} \boldsymbol{A}_{q,r}^p \cdot \boldsymbol{E}_q^p, \tag{56}$$

with

$$\begin{aligned} \boldsymbol{A}_0 &= \left[c_0 \boldsymbol{\mathcal{I}} + \sum_{i=1}^{2} c_i \boldsymbol{T}_i \right]^{-1}, & \boldsymbol{A}_s &= \boldsymbol{T}_s \cdot \boldsymbol{A}_0, \\ \boldsymbol{A}_{q,0}^p &= -\boldsymbol{A}_0 \cdot \sum_{i=1}^{2} c_i \boldsymbol{T}_{q,i}^p, & \boldsymbol{A}_{q,s}^p &= \boldsymbol{T}_{q,s}^p - \boldsymbol{A}_s \cdot \sum_{i=1}^{2} c_i \boldsymbol{T}_{q,i}^p, \end{aligned} \tag{57}$$

for $q = 0, 1, 2$ and $s = 1, 2$. In the above expression, $\boldsymbol{\mathcal{I}}$ is the 12×12 identity matrix. Moreover, combining equations (20), (56), (57) and $(54)_2$, yields

$$\overline{\boldsymbol{\Sigma}} = \overline{\boldsymbol{\mathcal{L}}} \cdot [\overline{\boldsymbol{E}} - \overline{\boldsymbol{E}}^p], \tag{58}$$

with

$$\begin{aligned} \overline{\boldsymbol{\mathcal{L}}} &= \sum_{i=0}^{2} c_i \boldsymbol{\mathcal{L}}_i \cdot \boldsymbol{A}_i, \quad \overline{\boldsymbol{E}}^p = \sum_{q=0}^{2} \boldsymbol{\mathcal{A}}_q^p \cdot \boldsymbol{E}_q^p, \\ \boldsymbol{\mathcal{A}}_q^p &= \overline{\boldsymbol{\mathcal{L}}}^{-1} \cdot \left[c_q \boldsymbol{\mathcal{L}}_q - \sum_{i=0}^{2} c_i \boldsymbol{\mathcal{L}}_i \cdot \boldsymbol{A}_{q,i}^p \right]. \end{aligned} \tag{59}$$

It is worth noting that non-uniform distributions of fibers can be accounted for by introducing appropriate orientation distribution functions in the expressions (57) and (59). One should bear in mind that the Mori-Tanaka scheme for reinforced composites with non-uniform alignment may lead to non-symmetric macroscopic magneto-electro-mechanical matrix $\overline{\boldsymbol{\mathcal{L}}}$. The symmetry issue could be potentially resolved by choosing another mean-field approach with similar structure, for example the Castañeda and Willis method (Ponte-Castañeda and Willis, 1995; Giordano, 2017). The latter assumes a unified ellipsoidal shape for the distribution of heterogeneities, which provides a consistent homogenization scheme and ensures the symmetry of the macroscopic matrix $\overline{\boldsymbol{\mathcal{L}}}$ for non-uniform alignment of the fibers.

4. Numerical applications

The purpose of this section is to demonstrate the developed micromechanics technique capabilities. For the needs of the numerical examples, four different materials are examined: $CoFe_2O_4$, $BaTiO_3$, glass and epoxy. The first one exhibits piezomagnetic behaviour, the second has piezoelectric characteristics and the last two present a typical mechanical response without magnetomechanical or electromechanical couplings. The material parameters of these materials are summarized in Table 1.

	$CoFe_2O_4$	$BaTiO_3$	glass	epoxy
n [GPa]	269.5	162	88.8	5.53
l [GPa]	170.5	78	29.6	2.97
K^{tr} [GPa]	229.5	121.5	59.2	4.25
μ^{tr} [GPa]	56.5	44.5	29.6	1.28
μ^{ax} [GPa]	45.3	43	29.6	1.28
κ^e_{11} [C^2/N m^2]	$0.8\cdot10^{-10}$	$112\cdot10^{-10}$	$0.56\cdot10^{-10}$	$1\cdot10^{-10}$
κ^e_{33} [C^2/N m^2]	$0.93\cdot10^{-10}$	$126\cdot10^{-10}$	$0.56\cdot10^{-10}$	$1\cdot10^{-10}$
κ^m_{11} [N/A^2]	$-590\cdot10^{-6}$	$5\cdot10^{-6}$	$1\cdot10^{-6}$	$1\cdot10^{-6}$
κ^m_{33} [N/A^2]	$157\cdot10^{-6}$	$10\cdot10^{-6}$	$1\cdot10^{-6}$	$1\cdot10^{-6}$
e_{31} [C/m^2]	0	-4.4	0	0
e_{33} [C/m^2]	0	18.6	0	0
e_{15} [C/m^2]	0	11.6	0	0
f_{31} [N/Am]	580.3	0	0	0
f_{33} [N/Am]	699.7	0	0	0
f_{15} [N/Am]	550	0	0	0
j_{11} [C/Am]	0	0	0	0
j_{33} [C/Am]	0	0	0	0

Table 1: Electro-magneto-mechanical properties for the materials utilized in the numerical examples. The properties of $CoFe_2O_4$, $BaTiO_3$ and epoxy have been obtained from Lee et al. (2005). The material parameters for the glass have been obtained from Dinzart and Sabar (2011).

4.1. Validation

In the first subsection, the electro-magneto-elastic properties of long fibers composites with and without coating layer are computed with the proposed method and are compared with the predictions of other methods in the literature.

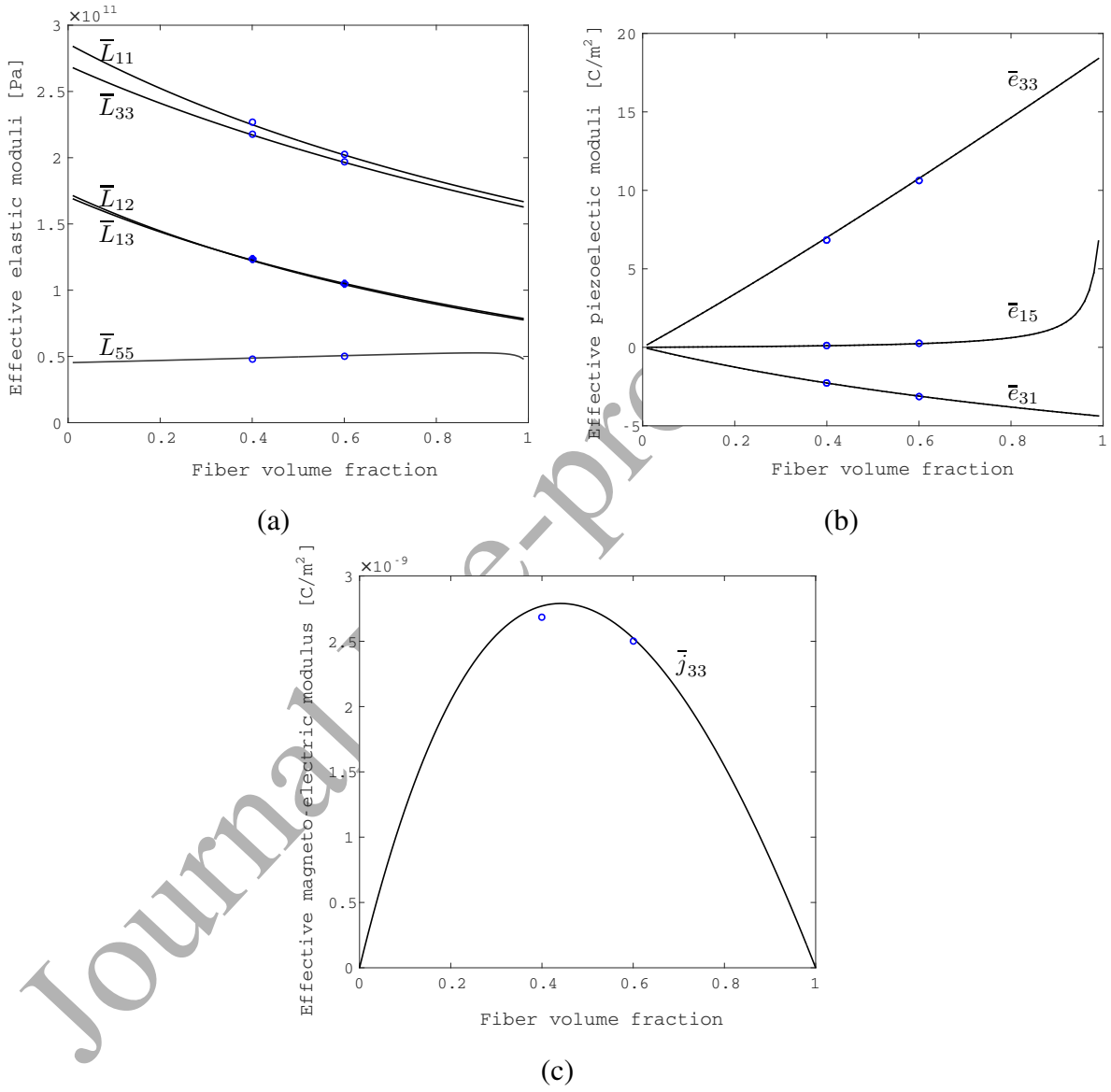

Figure 8: Material properties as a function of the fiber volume fraction for a composite consisting of $CoFe_2O_4$ matrix and $BaTiO_3$ long fibers: (a) mechanical, (b) piezoelectric and (c) electromagnetic coefficients. Comparison of the developed method predictions (solid lines) with numerical results obtained by Lee et al. (2005) (points).

In the first example, a composite consisting of $CoFe_2O_4$ matrix and $BaTiO_3$ long fibers is analyzed and the results are compared with the periodic homogenization predictions provided by Lee et al. (2005). The mechanical stiffness coefficients, the piezoelectric coupling terms and the electromagnetic coupling terms are demonstrated in Figure 8 as a function of the fiber volume fraction. The numerical results for the periodic homogenization analyses have been obtained only for two different volume fractions, 40% and 60% percent. As it can be observed, the new model simulations are in excellent agreement with the full field homogenization results.

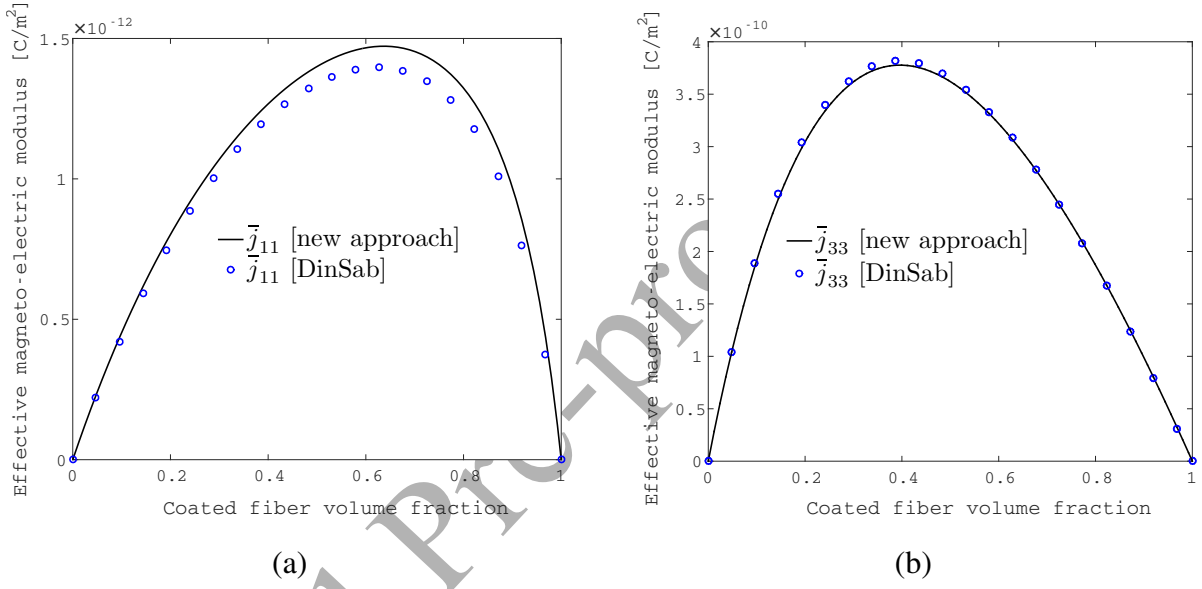

Figure 9: Electromagnetic properties as a function of the coated fiber volume fraction of a composite consisting of $CoFe_2O_4$ matrix and glass fibers coated with $BaTiO_3$ coating layer: Comparison of the developed method predictions (solid lines) with numerical results obtained by Dinzart and Sabar (2011) (points).

The second example illustrates results from studies in Dinzart and Sabar (2011). In that paper, an Eshelby-based micromechanics technique was developed using the Hill's interfacial operators. In their analysis, glass fibers coated with $BaTiO_3$ coating layer are embedded in $CoFe_2O_4$ matrix. The aspect ratio of the fibers (length to radius diameter) is 100, which is quite large and can serve for the purpose of this paper as almost long fiber. The ratio ϕ for the coated fibers is taken equal to 82.645%. Figure 9 illustrates the electromagnetic coupling terms of the composite as a function of the fiber volume fraction. The results of both methods are in good agreement and the small

difference is mainly due to the finite value of the fibers' aspect ratio.

The above preliminary examples demonstrate that the new approach has the same accuracy with existing homogenization techniques in terms of electro-magneto-mechanical properties. The following numerical studies demonstrate the ability of the model to predict both macroscopic and average microscopic fields per phase when nonlinear fields take place.

4.2. Applied thermal strains

A typical example of inelastic deformation is the appearance of thermal strains. Consider a composite made of $CoFe_2O_4$ matrix and glass fibers coated with $BaTiO_3$ coating layer. The composite is assumed free from external loading and only a temperature difference of 1 K is applied. The thermal expansion coefficients for the matrix, the fiber and the coating are taken equal to 10^{-5} 1/K, $5 \cdot 10^{-6}$ 1/K and $6.4 \cdot 10^{-6}$ 1/K respectively.

According to the general principles of homogenization of composites subjected to thermomechanical processes, the microscopic and macroscopic temperature coincide (Chatzigeorgiou et al., 2018), i.e. all material phases in the RVE are subjected to the same temperature difference of 1 K. This leads to the development of inelastic (thermal) strains in all phases:

$$\begin{aligned}
\boldsymbol{\varepsilon}_0^p &= \begin{bmatrix} 10^{-5} & 10^{-5} & 10^{-5} & 0 & 0 & 0 \end{bmatrix}^T, \\
\boldsymbol{\varepsilon}_1^p &= \begin{bmatrix} 5 \cdot 10^{-6} & 5 \cdot 10^{-6} & 5 \cdot 10^{-6} & 0 & 0 & 0 \end{bmatrix}^T, \\
\boldsymbol{\varepsilon}_2^p &= \begin{bmatrix} 6.4 \cdot 10^{-6} & 6.4 \cdot 10^{-6} & 6.4 \cdot 10^{-6} & 0 & 0 & 0 \end{bmatrix}^T.
\end{aligned}$$

Figure 10 illustrates the non zero terms of the macroscopic stress tensor, the electric displacement vector and the magnetic induction vector that are generated due to the thermal strains as a function of the fiber volume fraction. Considering the coating, two different ratios ϕ are considered: $\phi = 50\%$ and $\phi = 80\%$. From these results one observes that the stresses and the magnetic induction increase with the increase of c_1, while the electric displacement initially has a small increase and then decreases as the fiber volume fraction obtains high values.

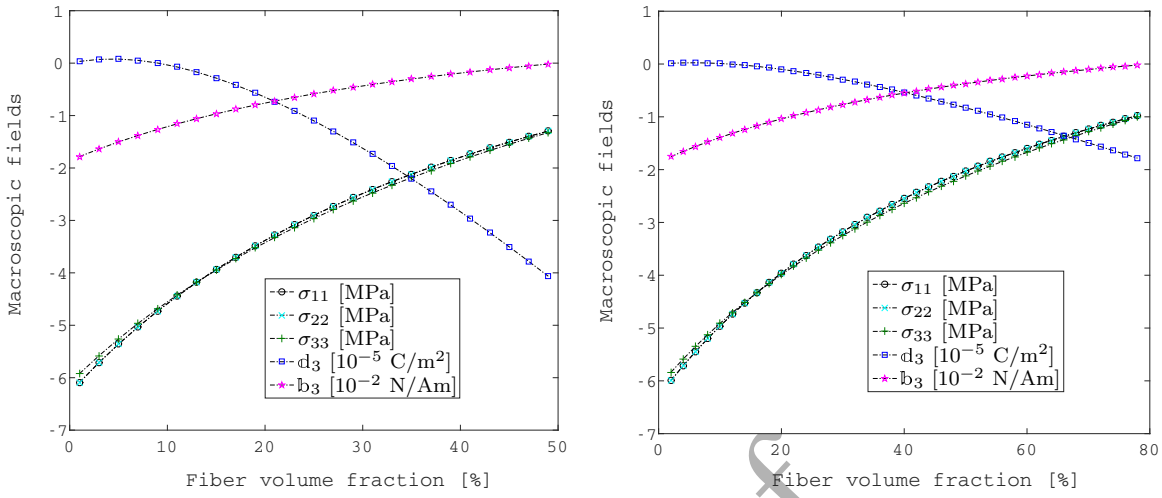

Figure 10: Composite consisting of $CoFe_2O_4$ matrix and glass fibers coated with $BaTiO_3$ coating layer. Macroscopic stress, electric displacement and magnetic induction fields, caused by thermal strains: (a) ratio $\phi = 50\%$ and (b) ratio $\phi = 80\%$.

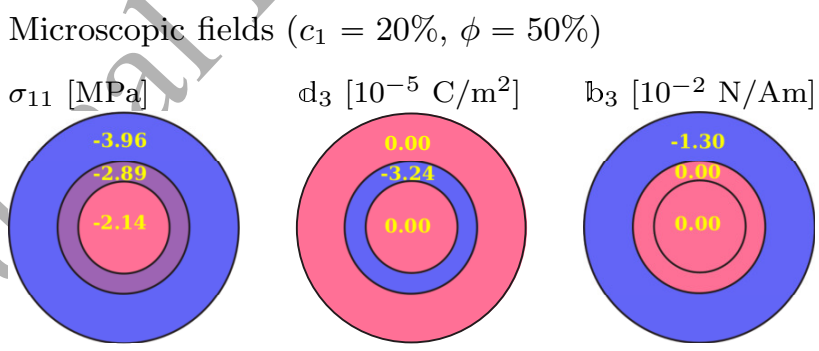

Figure 11: Composite consisting of $CoFe_2O_4$ matrix and glass fibers coated with $BaTiO_3$ coating layer. Average microscopic stress, electric displacement and magnetic induction fields per phase, caused by thermal strains, for fiber volume fraction 20% and ratio $\phi = 50\%$.

The average microscopic fields per phase for fiber volume fraction 20% and ratio $\phi = 50\%$ are demonstrated in Figure 11. As it can be observed, the electric displacement for the matrix and the fiber are zero. This phenomenon is explained by the structure of the interaction tensors (40) and the constitutive relations (8). The terms $\boldsymbol{T}^{e0}$ and $\boldsymbol{T}^{pe0}$ are linked with the development of electric fields inside the fiber and the coating due to the presence of mechanical strains. Similarly, the terms $\boldsymbol{T}^{m0}$ and $\boldsymbol{T}^{pm0}$ are linked with the development of magnetic fields inside the fiber and the coating due to the presence of mechanical strains. As it can be seen by the expressions (43), (44), (45) and (46) for these terms, elastic or inelastic normal strains cannot produce electric or magnetic field in the phases. Thus, according to the constitutive law relations (8), the development of electric displacement can appear only in phases with non zero piezoelectric coupling tensor $\boldsymbol{e}$, as it is the case for the coating ($BaTiO_3$). The glass and the $CoFe_2O_4$ have zero piezoelectric coefficients, and thus no electric field can be generated in these materials under only thermal strain conditions. For completely analogous reasons, magnetic induction can only be generated in the matrix ($CoFe_2O_4$) and not in the fiber or the coating. Contrarily to the microscopic scale, electric displacement and magnetic induction parallel to the fiber axis direction are generated at the macroscopic response, as it has already been shown in Figure 10.

4.3. Applied inelastic fields

Thermal strains are a special case of eigenfields. When nonlinear mechanisms like plasticity are activated, the mechanical inelastic strains may appear only on certain phases and do not act as a volumetric expansion.

Consider a composite consisting of epoxy matrix and $CoFe_2O_4$ fibers coated with $BaTiO_3$ coating layer. For this material system, two specific cases where the matrix phase is subjected to inelastic strains are discussed:

- Case 1: Inelastic normal strains $\varepsilon^p_{11_0} = -2\varepsilon^p_{22_0} = -2\varepsilon^p_{33_0} = 0.001$.

  Figure 12 shows the macroscopic and average microscopic responses of the investigated composite under inelastic normal strains in the matrix. The evolution of the macroscopic normal stresses, axial electric displacement and axial magnetic induction with respect to the

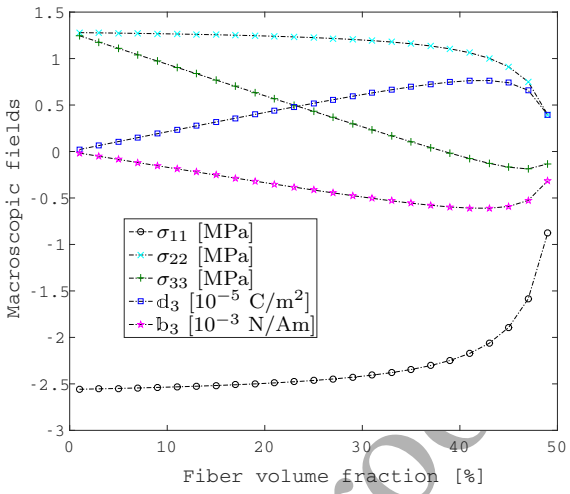

(a)

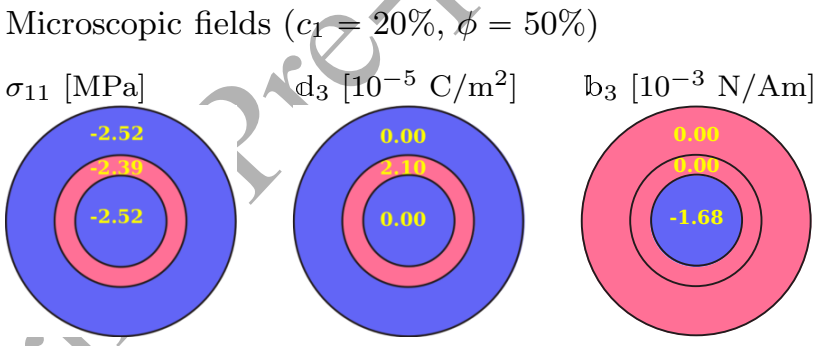

(b)

Figure 12: Composite consisting of epoxy matrix and $CoFe_2O_4$ fibers coated with $BaTiO_3$ coating layer, subjected to inelastic normal strains. Stress, electric displacement and magnetic induction, caused by inelastic normal strains, for ratio $\phi = 50\%$: (a) macroscopic fields and (b) average microscopic fields per phase for fiber volume fraction 20%.

fiber volume fraction c_1 is illustrated in Figure 12_a for ratio $\phi = 50\%$. It can be noticed that all macroscopic fields present significant change tendency at very high fiber volume fractions (i.e., when the matrix volume fraction is close to zero). For the microscopic fields (Figure 12_b), similar results to those of the previous study (presence of thermal strains) are observed. Thus, electric displacement and magnetic induction parallel to the fiber axis direction are generated only in phases where piezoelectric and piezomagnetic coupling terms, respectively, are non zero.

- Case 2: Inelastic shear strain $\varepsilon^p_{13_0} = 0.001$.

  Figure 13 shows the macroscopic and average microscopic responses of the investigated composite under inelastic axial shear strains in the matrix. The evolution of the macroscopic axial shear stress, transverse electric displacement and transverse magnetic induction with respect to the fiber volume fraction c_1 is given in Figure 13_a for ratio $\phi = 50\%$. It can be noticed that all macroscopic fields present significant change tendency at very high fiber volume fractions (i.e., when the matrix volume fraction is close to zero). For the microscopic fields (Figure 13_b) one observes that all phases experience electric displacement and magnetic induction. This is explained by the fact that, according to the interaction tensors forms (43), (44), (45) and (46), axial shear strain can activate electric and magnetic field. Thus, electric displacement and magnetic induction can also be generated in phases where electromechanical or magnetomechanical couplings do not exist.

5. Concluding comments

A micromechanical method was proposed for the evaluation of the electro-magneto-inelastic properties of coated long fiber composites with transversely isotropic piezoelectric-piezomagnetic behaviour. The method was based on solving specific boundary value problems (axial shear/in plane electric and magnetic field, transverse shear strain, plane strain/axial electric and magnetic field, hydrostatic strain/axial inelastic strain) and was adapted to the Mori-Tanaka homogenization scheme. The capabilities of the proposed micromechanics technique were verified through several

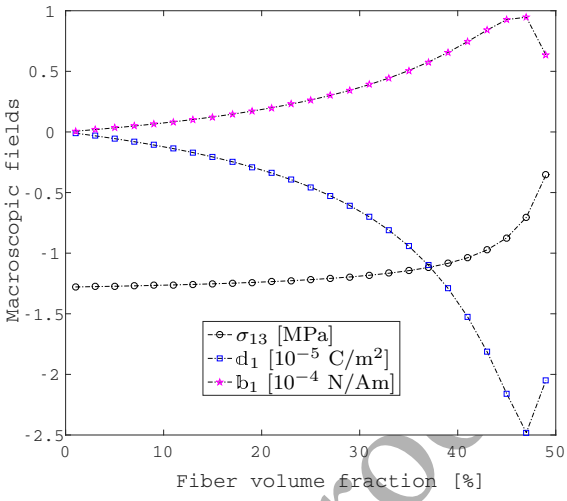

(a)

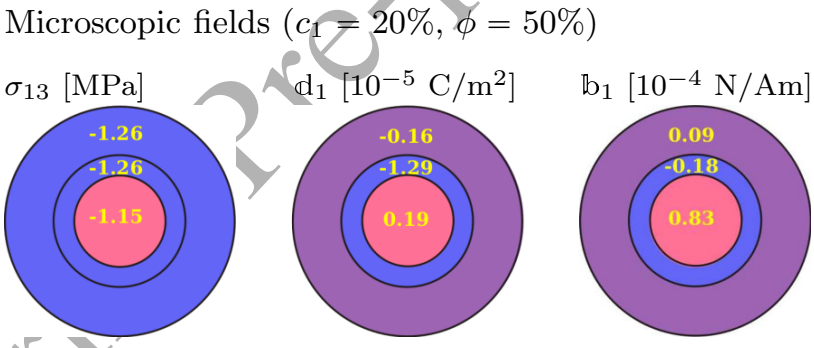

(b)

Figure 13: Composite consisting of epoxy matrix and $CoFe_2O_4$ fibers coated with $BaTiO_3$ coating layer, subjected to inelastic normal strains. Stress, electric displacement and magnetic induction, caused by inelastic axial shear strains, for ratio $\phi = 50\%$: (a) macroscopic fields and (b) average microscopic fields per phase for fiber volume fraction 20%.

numerical applications. Four materials with different behaviours have been examined ($CoFe_2O_4$ as a piezomagnetic material, $BaTiO_3$ as a piezoelectric material and both glass and epoxy as mechanical material without magneto- or electro-mechanical coupling) for the needs of the numerical applications. A comparison with existing homogenization techniques in terms of electro-magneto-mechanical properties of long fiber composites was first conducted. The simulation results of the proposed approach were in good agreement with the full field homogenization results. Small difference has been observed when comparing the electromagnetic coupling terms with studies conducted by Dinzart and Sabar (2011). This difference was mainly attributed to the finite value of the fibers' aspect ratio. The ability of the model to predict both macroscopic and average microscopic fields per phase when nonlinear fields are activated was then demonstrated. Three cases of applied inelastic fields were considered: thermal strains, inelastic normal strains and inelastic shear strains. The effect of the inelastic fields on the overall response, as well as in the average response of the phases, was then explicitly investigated. The proposed micromechanics approach is able to handle microstructures with aligned or non-aligned fiber composites with piezoelectric-piezomagnetic behaviour under inelasticity conditions.

A. Computational steps for obtaining the interaction tensors

The unknown constants $\Xi_{q,i}$ and $Z_{q,i}$ of the boundary value problems presented in subsection 3.2 are identified using i) the boundary conditions at $r = r_{\text{ext}} \to \infty$, ii) the consistency condition that the fields should be finite at $r = 0$, and iii) the interface conditions (25) and (26) between the material phases.

Before presenting the solution of the four boundary value problems, the following helpful matrices and vectors are introduced: Let's consider an arbitrary material parameter ω. For the

three phases this parameter becomes ω_q for $q = 0, 1, 2$. The next matrices and vectors

$$\boldsymbol{K}_\omega = \begin{bmatrix} 1 & -1 & -1 & 0 \\ \omega_1 & -\omega_2 & \omega_2 & 0 \\ 0 & 1 & \phi & -\phi \\ 0 & \omega_2 & -\omega_2\phi & \omega_0\phi \end{bmatrix}, \quad \boldsymbol{K}_\omega^{\mathrm{mix}} = \begin{bmatrix} 0 & 0 & 0 & 0 \\ \omega_1 & -\omega_2 & \omega_2 & 0 \\ 0 & 0 & 0 & 0 \\ 0 & \omega_2 & -\omega_2\phi & \omega_0\phi \end{bmatrix}, \tag{A.1}$$

$$\boldsymbol{F}_\omega = \begin{bmatrix} 0 \\ 0 \\ 1 \\ \omega_0 \end{bmatrix}, \ \boldsymbol{F}_\omega^{\mathrm{mix}} = \begin{bmatrix} 0 \\ 0 \\ 0 \\ \omega_0 \end{bmatrix}, \ \boldsymbol{F}_\omega^0 = \begin{bmatrix} 0 \\ 0 \\ 0 \\ -\omega_0 \end{bmatrix}, \ \boldsymbol{F}_\omega^1 = \begin{bmatrix} 0 \\ \omega_1 \\ 0 \\ 0 \end{bmatrix}, \ \boldsymbol{F}_\omega^2 = \begin{bmatrix} 0 \\ -\omega_2 \\ 0 \\ \omega_2 \end{bmatrix}, \tag{A.2}$$

have general description for the arbitrary ω and they become specific, once the ω_q are assigned to proper material parameters.

A.1. Axial shear / in-plane electric and magnetic field

For this boundary value problem, the boundary conditions and the fact that all fields should be finite at $r = 0$ yield

$$\Xi_{1,2} = \Xi^e_{1,2} = \Xi^m_{1,2} = 0, \quad \Xi_{0,1} = \beta, \quad \Xi^e_{0,1} = \beta^e, \quad \Xi^m_{0,1} = \beta^m. \tag{A.3}$$

The rest of unknown constants are given by the solution of the system

$$\breve{\boldsymbol{K}}_{xz} \cdot \breve{\boldsymbol{\Xi}} = \beta \breve{\boldsymbol{F}}_{xz} + \beta^e \breve{\boldsymbol{F}}^e_{xz} + \beta^m \breve{\boldsymbol{F}}^m_{xz} + \sum_{q=0}^{2} \left[s_q \breve{\boldsymbol{F}}^{p,q}_{xz} + s^e_q \breve{\boldsymbol{F}}^{pe,q}_{xz} + s^m_q \breve{\boldsymbol{F}}^{pm,q}_{xz} \right], \tag{A.4}$$

where

$$\breve{\boldsymbol{\Xi}} = \begin{bmatrix} \boldsymbol{\Xi} \\ \boldsymbol{\Xi}^e \\ \boldsymbol{\Xi}^m \end{bmatrix}, \quad \breve{\boldsymbol{F}}_{xz} = \begin{bmatrix} \boldsymbol{F}_{xz} \\ \boldsymbol{F}^e_{xz} \\ \boldsymbol{F}^m_{xz} \end{bmatrix}, \quad \breve{\boldsymbol{F}}^e_{xz} = \begin{bmatrix} -\boldsymbol{F}^e_{xz} \\ \boldsymbol{F}^{ee}_{xz} \\ \boldsymbol{F}^{em}_{xz} \end{bmatrix}, \quad \breve{\boldsymbol{F}}^m_{xz} = \begin{bmatrix} -\boldsymbol{F}^m_{xz} \\ \boldsymbol{F}^{em}_{xz} \\ \boldsymbol{F}^{mm}_{xz} \end{bmatrix}, \tag{A.5}$$

$$\breve{\boldsymbol{F}}_{xz}^{p,q} = \begin{bmatrix} \boldsymbol{F}_{xz}^{p,q} \\ \boldsymbol{F}_{xz}^{pe,q} \\ \boldsymbol{F}_{xz}^{pm,q} \end{bmatrix}, \quad \breve{\boldsymbol{F}}_{xz}^{pe,q} = \begin{bmatrix} -\boldsymbol{F}_{xz}^{pe,q} \\ \boldsymbol{F}_{xz}^{pee,q} \\ \boldsymbol{F}_{xz}^{pem,q} \end{bmatrix}, \quad \breve{\boldsymbol{F}}_{xz}^{pm,q} = \begin{bmatrix} -\boldsymbol{F}_{xz}^{pm,q} \\ \boldsymbol{F}_{xz}^{pem,q} \\ \boldsymbol{F}_{xz}^{pmm,q} \end{bmatrix}, \tag{A.6}$$

and

$$\breve{\boldsymbol{K}}_{xz} = \begin{bmatrix} \boldsymbol{K}_{xz} & -\boldsymbol{K}_{xz}^{e} & -\boldsymbol{K}_{xz}^{m} \\ \boldsymbol{K}_{xz}^{e} & \boldsymbol{K}_{xz}^{ee} & \boldsymbol{K}_{xz}^{em} \\ \boldsymbol{K}_{xz}^{m} & \boldsymbol{K}_{xz}^{em} & \boldsymbol{K}_{xz}^{mm} \end{bmatrix}, \tag{A.7}$$

with

$$\boldsymbol{\Xi} = \begin{bmatrix} \Xi_{1,1} \\ \Xi_{2,1} \\ \Xi_{2,2} \\ \Xi_{0,2} \end{bmatrix}, \quad \boldsymbol{\Xi}^{e} = \begin{bmatrix} \Xi_{1,1}^{e} \\ \Xi_{2,1}^{e} \\ \Xi_{2,2}^{e} \\ \Xi_{0,2}^{e} \end{bmatrix}, \quad \boldsymbol{\Xi}^{m} = \begin{bmatrix} \Xi_{1,1}^{m} \\ \Xi_{2,1}^{m} \\ \Xi_{2,2}^{m} \\ \Xi_{0,2}^{m} \end{bmatrix}. \tag{A.8}$$

The various vectors and matrices are given in Table A.1

The solution of this system can be written in the form

$$\breve{\boldsymbol{\Xi}} = \beta\breve{\boldsymbol{\Xi}}_{\text{mec}} + \beta^{e}\breve{\boldsymbol{\Xi}}_{\text{elc}} + \beta^{m}\breve{\boldsymbol{\Xi}}_{\text{mag}} + \sum_{q=0}^{2}\left[s_q\breve{\boldsymbol{\Xi}}_{\text{mec}}^{p,q} + s_q^{e}\breve{\boldsymbol{\Xi}}_{\text{elc}}^{p,q} + s_q^{m}\breve{\boldsymbol{\Xi}}_{\text{mag}}^{p,q}\right], \tag{A.9}$$

which can be split in three parts,

$$\begin{aligned}
\boldsymbol{\Xi} &= \beta\boldsymbol{\Xi}_{\text{mec}} + \beta^{e}\boldsymbol{\Xi}_{\text{elc}} + \beta^{m}\boldsymbol{\Xi}_{\text{mag}} + \sum_{q=0}^{2}\left[s_q\boldsymbol{\Xi}_{\text{mec}}^{p,q} + s_q^{e}\boldsymbol{\Xi}_{\text{elc}}^{p,q} + s_q^{m}\boldsymbol{\Xi}_{\text{mag}}^{p,q}\right], \\
\boldsymbol{\Xi}^{e} &= \beta\boldsymbol{\Xi}_{\text{mec}}^{e} + \beta^{e}\boldsymbol{\Xi}_{\text{elc}}^{e} + \beta^{m}\boldsymbol{\Xi}_{\text{mag}}^{e} + \sum_{q=0}^{2}\left[s_q\boldsymbol{\Xi}_{\text{mec}}^{pe,q} + s_q^{e}\boldsymbol{\Xi}_{\text{elc}}^{pe,q} + s_q^{m}\boldsymbol{\Xi}_{\text{mag}}^{pe,q}\right], \\
\boldsymbol{\Xi}^{m} &= \beta\boldsymbol{\Xi}_{\text{mec}}^{m} + \beta^{e}\boldsymbol{\Xi}_{\text{elc}}^{m} + \beta^{m}\boldsymbol{\Xi}_{\text{mag}}^{m} + \sum_{q=0}^{2}\left[s_q\boldsymbol{\Xi}_{\text{mec}}^{pm,q} + s_q^{e}\boldsymbol{\Xi}_{\text{elc}}^{pm,q} + s_q^{m}\boldsymbol{\Xi}_{\text{mag}}^{pm,q}\right].
\end{aligned} \tag{A.10}$$

The average strains, electric fields and magnetic fields in the fiber and the coating are given by

$$\begin{aligned}
\boldsymbol{\varepsilon}_i &= \Lambda_{xz}^{i}\begin{bmatrix} 0 & 0 & 0 & 0 & 1 & 0 \end{bmatrix}^{T}, \\
\mathfrak{e}_i &= \Lambda_{xz}^{e,i}\begin{bmatrix} 1 & 0 & 0 \end{bmatrix}^{T}, \\
\mathbb{h}_i &= \Lambda_{xz}^{m,i}\begin{bmatrix} 1 & 0 & 0 \end{bmatrix}^{T}, \quad i = 1, 2,
\end{aligned} \tag{A.11}$$

	ω					
	μ^{ax}	e_{15}	f_{15}	κ^e_{11}	κ^m_{11}	j_{11}
$\boldsymbol{K}_\omega$	$\boldsymbol{K}_{xz}$			$\boldsymbol{K}^{ee}_{xz}$	$\boldsymbol{K}^{mm}_{xz}$	
$\boldsymbol{K}^{\mathrm{mix}}_\omega$		$\boldsymbol{K}^{e}_{xz}$	$\boldsymbol{K}^{m}_{xz}$			$\boldsymbol{K}^{em}_{xz}$
$\boldsymbol{F}_\omega$	$\boldsymbol{F}_{xz}$			$\boldsymbol{F}^{ee}_{xz}$	$\boldsymbol{F}^{mm}_{xz}$	
$\boldsymbol{F}^{\mathrm{mix}}_\omega$		$\boldsymbol{F}^{e}_{xz}$	$\boldsymbol{F}^{m}_{xz}$			$\boldsymbol{F}^{em}_{xz}$
$\boldsymbol{F}^{q}_\omega$	$\boldsymbol{F}^{p,q}_{xz}$	$\boldsymbol{F}^{pe,q}_{xz}$	$\boldsymbol{F}^{pm,q}_{xz}$	$\boldsymbol{F}^{pee,q}_{xz}$	$\boldsymbol{F}^{pmm,q}_{xz}$	$\boldsymbol{F}^{pem,q}_{xz}$

Table A.1: Axial shear / in-plane electric and magnetic field: matrices and vectors used to compute the unknown constants. Each element in this table is computed by substituting to the general matrices or vectors a specific parameter for ω. The superscript q takes the value 0, 1 or 2.

with

$$\Lambda^1_{xz} = \Xi_{1,1}, \quad \Lambda^2_{xz} = \frac{\beta + [\Xi_{0,2} - \Lambda^1_{xz}]\phi}{1-\phi},$$
$$\Lambda^{e,1}_{xz} = \Xi^e_{1,1}, \quad \Lambda^{e,2}_{xz} = \frac{\beta^e + [\Xi^e_{0,2} - \Lambda^{e,1}_{xz}]\phi}{1-\phi},$$
$$\Lambda^{m,1}_{xz} = \Xi^m_{1,1}, \quad \Lambda^{m,2}_{xz} = \frac{\beta^m + [\Xi^m_{0,2} - \Lambda^{m,1}_{xz}]\phi}{1-\phi}. \tag{A.12}$$

The Λ^i_{xz}, $\Lambda^{e,i}_{xz}$ and $\Lambda^{m,i}_{xz}$ can be expressed in the same forms as (A.10).

A.2. Transverse shear

The boundary conditions and the fact that the displacement should be finite at $r = 0$ yield

$$\Xi_{1,3} = \Xi_{1,4} = \Xi_{0,1} = 0, \quad \Xi_{0,2} = \gamma. \tag{A.13}$$

The rest of unknown constants are given by the solution of the system

$$\boldsymbol{K}_{xy} \cdot \boldsymbol{\Xi} = \gamma \boldsymbol{F}_{xy} + \sum_{q=0}^{2} s_q \boldsymbol{F}^{p,q}_{xy}, \tag{A.14}$$

with

$$
\begin{aligned}
\boldsymbol{\Xi} &= \left[\begin{array}{cccccccc} \Xi_{1,1} & \Xi_{1,2} & \Xi_{2,1} & \Xi_{2,2} & \Xi_{2,3} & \Xi_{2,4} & \Xi_{0,3} & \Xi_{0,4} \end{array} \right]^T, \\
\boldsymbol{F}_{xy} &= \left[\begin{array}{cccccccc} 0 & 0 & 0 & 0 & 1 & 1 & 2\mu_0^{\mathrm{tr}} & 2\mu_0^{\mathrm{tr}} \end{array} \right]^T, \\
\boldsymbol{F}_{xy}^{p,0} &= \left[\begin{array}{cccccccc} 0 & 0 & 0 & 0 & 0 & 0 & -2\mu_0^{\mathrm{tr}} & -2\mu_0^{\mathrm{tr}} \end{array} \right]^T, \\
\boldsymbol{F}_{xy}^{p,1} &= \left[\begin{array}{cccccccc} 0 & 0 & 2\mu_1^{\mathrm{tr}} & 2\mu_1^{\mathrm{tr}} & 0 & 0 & 0 & 0 \end{array} \right]^T, \\
\boldsymbol{F}_{xy}^{p,2} &= \left[\begin{array}{cccccccc} 0 & 0 & -2\mu_2^{\mathrm{tr}} & -2\mu_2^{\mathrm{tr}} & 0 & 0 & 2\mu_2^{\mathrm{tr}} & 2\mu_2^{\mathrm{tr}} \end{array} \right]^T,
\end{aligned}
\tag{A.15}
$$

and

$$
\boldsymbol{K}_{xy} = \left[\begin{array}{cccccccc}
\psi_{1,1} & 1 & -\psi_{2,1} & -1 & 1 & -\psi_{2,4} & 0 & 0 \\
1 & 1 & -1 & -1 & -1 & -1 & 0 & 0 \\
K_{31} & K_{32} & K_{33} & K_{34} & K_{35} & K_{36} & 0 & 0 \\
K_{41} & K_{42} & K_{43} & K_{44} & K_{45} & K_{46} & 0 & 0 \\
0 & 0 & \psi_{2,1}/\phi & 1 & -\phi^2 & \psi_{2,4}\phi & \phi^2 & -\psi_{0,4}\phi \\
0 & 0 & 1/\phi & 1 & \phi^2 & \phi & -\phi^2 & -\phi \\
0 & 0 & K_{73} & K_{74} & K_{75} & K_{76} & K_{77} & K_{78} \\
0 & 0 & K_{83} & K_{84} & K_{85} & K_{86} & K_{87} & K_{88}
\end{array} \right],
\tag{A.16}
$$

with

$$
\begin{aligned}
K_{31} &= 2K_1^{\mathrm{tr}}[2\psi_{1,1} - 1] + 2\mu_1^{\mathrm{tr}}[1 + \psi_{1,1}], \quad K_{32} = 2\mu_1^{\mathrm{tr}}, \\
K_{33} &= -2K_2^{\mathrm{tr}}[2\psi_{2,1} - 1] - 2\mu_2^{\mathrm{tr}}[1 + \psi_{2,1}], \quad K_{34} = -2\mu_2^{\mathrm{tr}}, \\
K_{35} &= -6\mu_2^{\mathrm{tr}}, \quad K_{36} = 2\mu_2^{\mathrm{tr}}[\psi_{2,4} - 1] + 2K_2^{\mathrm{tr}},
\end{aligned}
$$

$$
\begin{aligned}
K_{41} &= 2\mu_1^{\mathrm{tr}}[1 + \psi_{1,1}], \quad K_{42} = 2\mu_1^{\mathrm{tr}}, \\
K_{43} &= -2\mu_2^{\mathrm{tr}}[1 + \psi_{2,1}], \quad K_{44} = -2\mu_2^{\mathrm{tr}}, \\
K_{45} &= 6\mu_2^{\mathrm{tr}}, \quad K_{46} = 2\mu_2^{\mathrm{tr}}[1 - \psi_{2,4}],
\end{aligned}
$$

$$
\begin{aligned}
K_{73} &= \left[2K_2^{\mathrm{tr}}[2\psi_{2,1}-1]+2\mu_2^{\mathrm{tr}}[1+\psi_{2,1}]\right]/\phi, \quad K_{74}=2\mu_2^{\mathrm{tr}},\\
K_{75} &= 6\mu_2^{\mathrm{tr}}\phi^2, \quad K_{76}=-\left[2\mu_2^{\mathrm{tr}}[\psi_{2,4}-1]+2K_2^{\mathrm{tr}}\right]\phi,\\
K_{77} &= -6\mu_0^{\mathrm{tr}}\phi^2, \quad K_{78}=\left[2\mu_0^{\mathrm{tr}}[\psi_{0,4}-1]+2K_0^{\mathrm{tr}}\right]\phi,
\end{aligned}
$$

$$
\begin{aligned}
K_{83} &= 2\mu_2^{\mathrm{tr}}[1+\psi_{2,1}]/\phi, \quad K_{84}=2\mu_2^{\mathrm{tr}},\\
K_{85} &= -6\mu_2^{\mathrm{tr}}\phi^2, \quad K_{86}=-2\mu_2^{\mathrm{tr}}[1-\psi_{2,4}]\phi,\\
K_{87} &= 6\mu_0^{\mathrm{tr}}\phi^2, \quad K_{88}=2\mu_0^{\mathrm{tr}}[1-\psi_{0,4}]\phi.
\end{aligned}
$$

The solution of this system can be written in the form

$$
\boldsymbol{\Xi} = \gamma\boldsymbol{\Xi}_{\mathrm{mec}}+\sum_{q=0}^{2} s_q\boldsymbol{\Xi}_{\mathrm{mec}}^{p,q}. \tag{A.17}
$$

The average strains in the fiber and the coating are given by

$$
\boldsymbol{\varepsilon}_i = 2\Lambda_{xy}^i\begin{bmatrix} 0 & 0 & 0 & 1 & 0 & 0\end{bmatrix}^T, \tag{A.18}
$$

with

$$
\Lambda_{xy}^1 = \frac{1+\psi_{1,1}}{2}\Xi_{1,1}+\Xi_{1,2}, \quad \Lambda_{xy}^2 = \frac{1}{1-\phi}\left[\gamma+\left[\frac{1+\psi_{0,4}}{2}\Xi_{0,4}-\Lambda_{xy}^1\right]\phi\right]. \tag{A.19}
$$

The Λ_{xy}^i can be expressed in the same form as (A.17).

A.3. Plane strain / axial electric and magnetic field

The boundary conditions and the fact that the displacement should be finite at $r=0$ yield

$$
\Xi_{1,3}=\Xi_{1,4}=\Xi_{0,1}=Z_{1,2}=0, \quad \Xi_{0,2}=\gamma, \quad Z_{0,1}=\beta. \tag{A.20}
$$

The rest of unknown constants are given by the solution of two systems:

1. The first is written as

$$
\boldsymbol{K}_{xx}\cdot\boldsymbol{Z} = \beta\boldsymbol{F}_{xx}+\beta^e\boldsymbol{F}_{xx}^e+\beta^m\boldsymbol{F}_{xx}^m+\sum_{q=0}^{2}\left[s_{q,\beta}\boldsymbol{F}_{xx}^{p,q}+s_q^e\boldsymbol{F}_{xx}^{pe,q}+s_q^m\boldsymbol{F}_{xx}^{pm,q}\right], \tag{A.21}
$$

with

$$
\boldsymbol{Z} = \begin{bmatrix} Z_{1,1} & Z_{2,1} & Z_{2,2} & Z_{0,2}\end{bmatrix}^T, \tag{A.22}
$$

$$\boldsymbol{F}_{xx} = \boldsymbol{F}_{\omega} \quad \text{and} \quad \boldsymbol{F}_{xx}^{p,q} = \boldsymbol{F}_{\omega}^{q} \quad \text{for} \quad \omega = 2K^{\text{tr}}, \tag{A.23}$$

$$\boldsymbol{F}_{xx}^{e} = \sum_{q=0}^{2} \boldsymbol{F}_{\omega}^{q} \quad \text{and} \quad \boldsymbol{F}_{xx}^{pe,q} = -\boldsymbol{F}_{\omega}^{q} \quad \text{for} \quad \omega = e_{31},$$

$$\boldsymbol{F}_{xx}^{m} = \sum_{q=0}^{2} \boldsymbol{F}_{\omega}^{q} \quad \text{and} \quad \boldsymbol{F}_{xx}^{pm,q} = -\boldsymbol{F}_{\omega}^{q} \quad \text{for} \quad \omega = f_{31}, \tag{A.24}$$

and

$$\boldsymbol{K}_{xx} = \begin{bmatrix} 1 & -1 & -1 & 0 \\ 2K_1^{\text{tr}} & -2K_2^{\text{tr}} & 2\mu_2^{\text{tr}} & 0 \\ 0 & 1 & \phi & -\phi \\ 0 & 2K_2 & -2\mu_2^{\text{tr}}\phi & 2\mu_0^{\text{tr}}\phi \end{bmatrix}. \tag{A.25}$$

The solution of this system can be written in the form

$$\boldsymbol{Z} = \beta \boldsymbol{Z}_{\text{mec}} + \beta^{e} \boldsymbol{Z}_{\text{elc}} + \beta^{m} \boldsymbol{Z}_{\text{mag}} + \sum_{q=0}^{2} \left[s_q \boldsymbol{Z}_{\text{mec}}^{p,q} + s_q^{e} \boldsymbol{Z}_{\text{elc}}^{p,q} + s_q^{m} \boldsymbol{Z}_{\text{mag}}^{p,q} \right]. \tag{A.26}$$

2. The second is written as

$$\boldsymbol{K}_{xy} \cdot \boldsymbol{\Xi} = \gamma \boldsymbol{F}_{xy} + \sum_{q=0}^{2} s_{q,\gamma} \boldsymbol{F}_{xy}^{p,q}, \tag{A.27}$$

where $\boldsymbol{\Xi}$, $\boldsymbol{F}_{xy}$, $\boldsymbol{F}_{xy}^{p,q}$ are given by (A.15) and $\boldsymbol{K}_{xy}$ is given by (A.16).

The average strains, electric fields and magnetic fields in the fiber and the coating are given by

$$\begin{aligned} \boldsymbol{\varepsilon}_i &= \Lambda_{xx}^{i} \begin{bmatrix} 1 & 1 & 0 & 0 & 0 & 0 \end{bmatrix}^{T} + \Lambda_{xy}^{i} \begin{bmatrix} 1 & -1 & 0 & 0 & 0 & 0 \end{bmatrix}^{T}, \\ \mathfrak{e}_i &= \beta^{e} \begin{bmatrix} 0 & 0 & 1 \end{bmatrix}^{T}, \quad \mathbb{h}_i = \beta^{m} \begin{bmatrix} 0 & 0 & 1 \end{bmatrix}^{T}, \end{aligned} \tag{A.28}$$

with

$$\Lambda_{xx}^{1} = Z_{1,1}, \quad \Lambda_{xx}^{2} = \frac{\beta + [Z_{0,2} - \Lambda_{xx}^{1}]\phi}{1 - \phi}, \tag{A.29}$$

and Λ_{xy}^{1}, Λ_{xy}^{2} are the same with those of the expressions (A.19). The Λ_{xx}^{i} can be expressed in the same form as (A.26).

A.4. Hydrostatic strain

For this boundary value problem, the boundary conditions and the fact that the displacement should be finite at $r = 0$ yield

$$Z_{1,2} = 0, \quad Z_{0,1} = \beta. \tag{A.30}$$

The rest of unknown constants are given by the solution of the system

$$\boldsymbol{K}_{xx} \cdot \boldsymbol{Z} = \beta \boldsymbol{F}_{zz} + \sum_{q=0}^{2} s_q \boldsymbol{F}_{zz}^{p,q}, \tag{A.31}$$

with

$$\boldsymbol{Z} = \begin{bmatrix} Z_{1,1} & Z_{2,1} & Z_{2,2} & Z_{0,2} \end{bmatrix}^T, \quad \boldsymbol{F}_{zz} = \begin{bmatrix} 0 & l_2 - l_1 & 1 & 2K_0^{\mathrm{tr}} + l_0 - l_2 \end{bmatrix}^T, \tag{A.32}$$

$$\boldsymbol{F}_{zz}^{p,q} = \boldsymbol{F}_{\omega}^{q} \quad \text{for} \quad \omega = l, \tag{A.33}$$

and $\boldsymbol{K}_{xx}$ is the same with (A.25). The solution of this system can be written in the form

$$\boldsymbol{Z} = \beta \boldsymbol{Z}_{\mathrm{mec}} + \sum_{q=0}^{2} s_r \boldsymbol{Z}_{\mathrm{mec}}^{p,q}. \tag{A.34}$$

The average strains in the fiber and the coating are given by

$$\boldsymbol{\varepsilon}_i = \beta \begin{bmatrix} \Lambda_{zz}^i & \Lambda_{zz}^i & 1 & 0 & 0 & 0 \end{bmatrix}^T, \tag{A.35}$$

with

$$\Lambda_{zz}^1 = Z_{1,1}, \quad \Lambda_{zz}^2 = \frac{\beta + [Z_{0,2} - \Lambda_{zz}^1]\phi}{1 - \phi}. \tag{A.36}$$

The Λ_{zz}^i can be expressed in the same form as (A.34).

A.5. Interaction tensors

Regrouping the results of the previous subsections, one finds that the interaction tensor components in (41)-(52) are given by the expressions

$$
\begin{aligned}
\left[T^i_{xx}\right]_{\text{mec}} &= \left[\Lambda^i_{xx}\right]_{\text{mec}}, & \left[T^i_{zz}\right]_{\text{mec}} &= \left[\Lambda^i_{zz}\right]_{\text{mec}},\\
\left[T^i_{xy}\right]_{\text{mec}} &= \left[\Lambda^i_{xy}\right]_{\text{mec}}, & \left[T^i_{xz}\right]_{\text{mec}} &= \left[\Lambda^i_{xz}\right]_{\text{mec}},\\
\left[T^{p,q,i}_{xx}\right]_{\text{mec}} &= \left[\Lambda^{p,q,i}_{xx}\right]_{\text{mec}}, & \left[T^{p,q,i}_{zz}\right]_{\text{mec}} &= \left[\Lambda^{p,q,i}_{zz}\right]_{\text{mec}},\\
\left[T^{p,q,i}_{xy}\right]_{\text{mec}} &= \left[\Lambda^{p,q,i}_{xy}\right]_{\text{mec}}, & \left[T^{p,q,i}_{xz}\right]_{\text{mec}} &= \left[\Lambda^{p,q,i}_{xz}\right]_{\text{mec}},\\
\left[T^{e,i}_{xz}\right]_{\text{mec}} &= -\left[\Lambda^{e,i}_{xz}\right]_{\text{mec}}, & \left[T^{pe,q,i}_{xz}\right]_{\text{mec}} &= -\left[\Lambda^{pe,q,i}_{xz}\right]_{\text{mec}},\\
\left[T^{m,i}_{xz}\right]_{\text{mec}} &= -\left[\Lambda^{m,i}_{xz}\right]_{\text{mec}}, & \left[T^{pm,q,i}_{xz}\right]_{\text{mec}} &= -\left[\Lambda^{pm,q,i}_{xz}\right]_{\text{mec}},\\
\left[T^i_{xx}\right]_{\text{elc}} &= -\left[\Lambda^i_{xx}\right]_{\text{elc}}, & \left[T^i_{xz}\right]_{\text{elc}} &= -\left[\Lambda^i_{xz}\right]_{\text{elc}},\\
\left[T^{p,q,i}_{xx}\right]_{\text{elc}} &= -\left[\Lambda^{p,q,i}_{xx}\right]_{\text{elc}}, & \left[T^{p,q,i}_{xz}\right]_{\text{elc}} &= -\left[\Lambda^{p,q,i}_{xz}\right]_{\text{elc}},\\
\left[T^i_{xx}\right]_{\text{mag}} &= -\left[\Lambda^i_{xx}\right]_{\text{mag}}, & \left[T^i_{xz}\right]_{\text{mag}} &= -\left[\Lambda^i_{xz}\right]_{\text{mag}},\\
\left[T^{p,q,i}_{xx}\right]_{\text{mag}} &= -\left[\Lambda^{p,q,i}_{xx}\right]_{\text{mag}}, & \left[T^{p,q,i}_{xz}\right]_{\text{mag}} &= -\left[\Lambda^{p,q,i}_{xz}\right]_{\text{mag}},\\
\left[T^{e,i}_{xz}\right]_{\text{elc}} &= \left[\Lambda^{e,i}_{xz}\right]_{\text{elc}}, & \left[T^{pe,q,i}_{xz}\right]_{\text{elc}} &= \left[\Lambda^{pe,q,i}_{xz}\right]_{\text{elc}},\\
\left[T^{m,i}_{xz}\right]_{\text{mag}} &= \left[\Lambda^{m,i}_{xz}\right]_{\text{mag}}, & \left[T^{pm,q,i}_{xz}\right]_{\text{mag}} &= \left[\Lambda^{pm,q,i}_{xz}\right]_{\text{mag}},\\
\left[T^{m,i}_{xz}\right]_{\text{elc}} &= \left[\Lambda^{m,i}_{xz}\right]_{\text{elc}}, & \left[T^{pm,q,i}_{xz}\right]_{\text{elc}} &= \left[\Lambda^{pm,q,i}_{xz}\right]_{\text{elc}},\\
\left[T^{e,i}_{xz}\right]_{\text{mag}} &= \left[\Lambda^{e,i}_{xz}\right]_{\text{mag}}, & \left[T^{pe,q,i}_{xz}\right]_{\text{mag}} &= \left[\Lambda^{pe,q,i}_{xz}\right]_{\text{mag}}.
\end{aligned}
\tag{A.37}
$$

References

References

Aboudi, J., 2001. Micromechanical analysis of fully coupled electro-magneto-thermo-elastic multiphase composites. Smart Materials and Structures 10, 867–877.

Akbarzadeh, A., Chen, Z., 2014. Thermo-Magneto-Electro-Elastic Responses of Rotating Hollow Cylinders. Mechanics of Advanced Materials and Structures 21, 67–80.

Benveniste, Y., 1995. Magnetoelectric effect in fibrous composites with piezoelectric and piezomagnetic phases. Physical Review B 51 (22), 16424–16427.

Benveniste, Y., Dvorak, G. J., Chen, T., 1989. Stress fields in composites with coated inclusions. Mechanics of Materials 7, 305–317.

Berbenni, S., Cherkaoui, M., 2010. Homogenization of multicoated inclusion-reinforced linear elastic composites with eigenstrains: Application to thermoelastic behavior. Philosophical Magazine 90 (22), 3003–3026.

Bishay, P. L., Atluri, S. N., 2016. Micromechanical Modeling of Piezoelectric-piezomagnetic Composites Using Computational Piezo-grains (CPGs). Materials Today: Proceedings 3, 167–172.

Bravo-Castillero, J., Rodríguez-Ramos, R., Mechkour, H., Otero, J. A., Cabanas, J. H., Sixto, L. M., Guinovart-Díaz, R., Sabina, F. J., 2009. Homogenization and effective properties of periodic thermomagnetoelectroelastic composites. Journal of Mechanics of Materials and Structures 4 (5), 819–836.

Bravo-Castillero, J., Rodríguez-Ramos, R., Mechkour, H., Otero, J. A., Sabina, F. J., 2008. Homogenization of magneto-electro-elastic multilaminated materials. The Quarterly Journal of Mechanics and Applied Mathematics 61 (3), 311–332.

Challagulla, K. S., Georgiades, A. V., 2011. Micromechanical analysis of magneto-electro-thermo-elastic composite materials with applications to multilayered structures. International Journal of Engineering Science 49, 85–104.

Chatzigeorgiou, G., Charalambakis, N., Chemisky, Y., Meraghni, F., 2018. Thermomechanical Behavior of Dissipative Composite Materials. ISTE Press - Elsevier, London.

Chatzigeorgiou, G., Javili, A., Meraghni, F., 2019. Micromechanical method for effective piezoelectric properties and electromechanical fields in multi-coated long fiber composites. International Journal of Solids and Structures 159, 21–39.

Chatzigeorgiou, G., Meraghni, F., 2019. Elastic and inelastic local strain fields in composites with coated fibers or particles: Theory and validation. Mathematics and Mechanics of Solids, in press.

Chatzigeorgiou, G., Seidel, G. D., Lagoudas, D. C., 2012. Effective mechanical properties of aligned "fuzzy fiber" composites. Composites Part B: Engineering, special issue "Homogenization and Micromechanics of Smart and Multifunctional Materials" 43, 2577–2593.

Cherkaoui, M., Sabar, H., Berveiller, M., 1995. Elastic composites with coated reinforcements: a micromechanical approach for nonhomothetic topology. Journal of Engineering Materials and Technology 33 (6), 829–843.

Christensen, R. M., 1979. Mechanics of composite materials. Dover, New York.

Dinzart, F., Sabar, H., 2011. Magneto-electro-elastic coated inclusion problem and its application to magnetic-piezoelectric composite materials. International Journal of Solids and Structures 48, 2393–2401.

Dunn, M. L., Taya, M., 1993. Micromechanics predictions of the effective electroelastic moduli of piezoelectric composites. International Journal of Solids and Structures 30 (2), 161–175.

Dvorak, G., Benveniste, Y., 1992. On transformation strains and uniform fields in multiphase elastic media. Proceedings of the Royal Society of London A 437, 291–310.

Eshelby, J. D., 1957. The Determination of the Elastic Field of an Ellipsoidal Inclusion, and Related Problems.

Proceedings of the Royal Society of London. Series A, Mathematical and Physical Sciences 241 (1226), 376–396.

Giordano, S., 2017. Nonlinear effective properties of heterogeneous materials with ellipsoidal microstructure. Mechanics of Materials 105, 16–28.

Hadjiloizi, D. A., Georgiades, A. V., Kalamkarov, A. L., Jothi, S., 2013. Micromechanical modeling of piezo-magneto-thermo-elastic composite structures: Part I - Theory. European Journal of Mechanics A/Solids 39, 298–312.

Hashin, Z., Rosen, B. W., 1964. The elastic moduli of fiber-reinforced materials. Journal of Applied Mechanics 31, 223–232.

Hill, R., 1983. Interfacial operators in the mechanics of composite media. Journal of the Mechanics and Physics of Solids 31 (4), 347–357.

Huang, J. H., Chiu, Y.-H., Liu, H.-K., 1998. Magneto-electro-elastic Eshelby tensors for a piezoelectric-piezomagnetic composite reinforced by ellipsoidal inclusions. Journal of Applied Physics 83, 5364.

Huang, J. H., Kuo, W.-S., 1997. The analysis of piezoelectric/piezomagnetic composite materials containing ellipsoidal inclusions. Journal of Applied Mechanics 81, 1378.

Koutsawa, Y., 2015. Overall thermo-magneto-electro-elastic properties of multiferroics composite materials with arbitrary heterogeneities spatial distributions. Composite Structures 133, 764–773.

Koutsawa, Y., Belouettar, S., Makradi, A., Tiem, S., 2011. Generalization of the micromechanics multi-coating approach to coupled fields composite materials with eigenfields: Effective properties. Mechanics Research Communications 38, 45–51.

Koutsawa, Y., Biscani, F., Belouettar, S., Nasser, H., Carrera, E., 2010. Multi-coating inhomogeneities approach for the effective thermo-electro-elastic properties of piezoelectric composite materials. Composite Structures 92, 964–972.

Kuo, H.-Y., Hsin, K.-C., 2018. Functionally graded piezoelectric-piezomagnetic fibrous composites. Acta Mechanica 229, 1503–1516.

Kuo, H.-Y., Peng, C.-Y., 2013. Magnetoelectricity in coated fibrous composites of piezoelectric and piezomagnetic phases. International Journal of Engineering Science 62, 70–83.

Lee, J., Boyd IV, J. G., Lagoudas, D. C., 2005. Effective properties of three-phase electro-magneto-elastic composites. International Journal of Engineering Science 43, 790–825.

Li, J. Y., 2000. Magnetoelectroelastic multi-inclusion and inhomogeneity problems and their applications in composite materials. International Journal of Engineering Science 38, 1993–2011.

Li, J. Y., Dunn, M. L., 1998. Micromechanics of Magnetoelectroelastic Composite Materials: Average Fields and Effective Behavior. Journal of Intelligent Material Systems and Structures 9, 404–416.

Nan, C.-W., 1994. Magnetoelectric effect in composites of piezoelectric and piezomagnetic phases. Physical Review B 50, 6082–6088.

Pakam, N., Arockiarajan, A., 2014. Study on effective properties of 1-3-2 type magneto-electro-elastic composites. Sensors and Actuators A: Physical 209, 87–99.

Payandeh, Y., Meraghni, F., Patoor, E., Eberhardt, A., 2010. Debonding initiation in a NiTi shape memory wire-epoxy matrix composite. Influence of martensitic transformation. Materials and Design 31, 1077–1084.

Payandeh, Y., Meraghni, F., Patoor, E., Eberhardt, A., 2012. Study of the martensitic transformation in NiTi-epoxy smart composite and its effect on the overall behavior. Materials and Design 39, 104–110.

Pettermann, H. E., Plankensteiner, A. F., Böhm, H. J., Rammerstorfer, F. G., 1999. A thermo-elasto-plastic constitutive law for inhomogeneous materials based on an incremental Mori-Tanaka approach. Computers and Structures 71, 197–214.

Ponte-Castañeda, P., Willis, J. R., 1995. The effect of spatial distribution on the effective behavior of composite materials and cracked media. Journal of the Mechanics and Physics of Solids 43 (12), 1919–1951.

Tang, T., Yu, W., 2009. Micromechanical modeling of the multiphysical behavior of smart materials using the variational asymptotic method. Smart Materials and Structures 18, 125026.

Walpole, L. J., 1978. A coated inclusion in an elastic medium. Mathematical Proceedings of the Cambridge Philosophical Society 83, 495–506.

Wang, Z., Oelkers, R. J., Lee, K. C., Fisher, F. T., 2016. Annular Coated Inclusion model and applications for polymer nanocomposites Part II: Cylindrical inclusions. Mechanics of Materials 101, 50–60.

Wu, T.-L., Huang, J. H., 2000. Closed-form solutions for the magnetoelectric coupling coefficients in fibrous composites with piezoelectric and piezomagnetic phases. International Journal of Solids and Structures 37, 2981–3009.

Ye, J., Cai, H., Wang, Y., Jing, Z., Shi, B., Qiu, Y., Chen, X., 2018. Effective mechanical properties of piezoelectric-piezomagnetic hybrid smart composites. Journal of Intelligent Material Systems and Structures 29, 1711–1723.